AMERICAN UNIVERSITY OF BEIRUT

WHAT IS THE EFFECT OF URBAN EMISSION OF ACID GASES (NO_2 AND SO_2) ON THE PHYSICAL AND CHEMICAL PROPERTIES OF AEROSOLS?

by
Lubna Maher Dada

A thesis
submitted in partial fulfillment of the requirements
for the degree of Master of Science
to the Department of Chemistry
of the Faculty of Arts and Sciences
at the American University of Beirut

Beirut, Lebanon
May 2014

AMERICAN UNIVERSITY OF BEIRUT

WHAT IS THE EFFECT OF URBAN EMISSION OF ACID GASES (NO_2 AND SO_2) ON THE PHYSICAL AND CHEMICAL PROPERTIES OF AEROSOLS?

by

LUBNA MAHER DADA

Approved by:

Dr. Najat A. Saliba, Professor
Chemistry — Advisor

Dr. Alan Louis Shihadeh, Professor
Mechanical Engineering — Member of Committee

Dr. Zeina Kassaify, Associate Professor
Nutrition & Food Sciences — Member of Committee

Date of thesis defense: May 16, 2014

AMERICAN UNIVERSITY OF BEIRUT

THESIS, DISSERTATION, PROJECT RELEASE FORM

Student Name: Dada Lubna Maher
Last First Middle

☑ Master's Thesis ○ Master's Project ○ Doctoral Dissertation

☑ I authorize the American University of Beirut to: (a) reproduce hard or electronic copies of my thesis, dissertation, or project; (b) include such copies in the archives and digital repositories of the University; and (c) make freely available such copies to third parties for research or educational purposes.

☐ I authorize the American University of Beirut, **three years after the date of submitting my thesis, dissertation, or project,** to: (a) reproduce hard or electronic copies of it; (b) include such copies in the archives and digital repositories of the University; and (c) make freely available such copies to third parties for research or educational purposes.

Signature May 19, 2014
Date

ACKNOWLEDGMENTS

I would like to devote my gratitude to my advisor Dr. Najat A Saliba for her exceptional guidance, constructive criticism, and patience over my two graduate years of research. I would like to thank her for her valuable advice and her encouragement to reach my maximum potential. I accredit my knowledge and the level of my instrumental experience to her assistance, and without her this thesis would not have been accomplished.

I would also like to give my appreciation to the committee members Dr. Alan Louis Shihadeh and Dr. Zeina Kassaify for her their helpful comments and guidance through this thesis.

I am, also, very thankful to Mr. Issam Saliba for teaching me that "Impossible is just an excuse".

Moreover, I would like to express my sincere acknowledgment to the efforts of the chemistry faculty and staff mainly; Mr. Issam Sleiman, Mr. Adnan Ruzz, Ms. Lama Shebani, and Mrs. Lara Abramian. I would also like to thank the CRSL staff including Ms. Rania Shatila, Mr. Joan Younes and Mr. Chady Assaf. I would like to thank the microbiology lab Ms. Reem Hamzeh and Ms. Mona al-Hasan.

I would like to thank Rima Baalbaki, for her backup plans, for her hard work and help throughout the whole thesis project, along with providing me with the friendliest atmosphere and support to carry out my research and field work. Also, I would like to thank Malik Jaafar, my partner in current and future crimes, for being there all the way, through the up and down, the dinner in town and the cap and gown. From the bottom of my heart, I would like to acknowledge Nour Naffaa for her warm and beautiful support through the toughest times. I would like to thank Lamis al Aaraj for her kind heart and friendliest care. Thank you Rita Tohme for your fun company and daily updates. Many thanks to my other friends who have shared this experience with me including Ms. Elizabeth Sepedjian, Ms. Joanne Klaiany, Mrs. Rachel el-Hajj, Mr. Ahmad Hellany and Mr. Hasan Harb along with the graduate students in the Chemistry department, the graduating, the struggling and the new.

I am blessed to have my childhood friends back me up all the way through my thesis writing, preparation and presentation. It has been more than ten years of a journey together and you never failed to support me no matter the circumstances. I acknowledge Rasha Majzoub, Reem Akra, Ali Jrady and Bilal Mekkawi for being there, ALWAYS, and no matter what. Also, I would like to thank Mohamed Nasreddine for his constant encouragement.

Also, I would like to devote this success to my loving family who proved to be the best anyone could ever wish for. The strength of my character and the person I am now are because of their constant ambition. To my dad, I hope I made you proud. I have only wished that you would be with me looking after me and holding me on your shoulders so that I reach the top of the world.

Finally, I owe this achievement to my mother, the love of my life, my sister and my super hero. No words are enough to express my gratitude for her making me the lady I am today. Her belief in my potential and abilities is the reason behind my accomplishments today.

AN ABSTRACT OF THE THESIS OF

Lubna Maher Dada for Master of Science
Major: Chemistry

Title: What is the effect of urban emission of acid gases (NO_2 and SO_2) on the physical and chemical properties of aerosols?

Beirut, which lies at the Eastern Mediterranean shore, is subject to two different types of dust storms. These dust storms, which are of Arabian or African origins and have different characteristics, result in an increase in total particulate matter concentration in the atmosphere. Atmospheric aerosols are subject to mixing with acid gases, anthropogenic pollution, and marine particles resulting in physical and chemical transformations of primary particles along with the formation of secondary ones.

Dust storms result in a total increase in the acidic gases HONO, HNO_3 and H_2SO_4. Along with the direct deposition effects on the environment, acidic gases influence the inorganic content of particulate matter; mainly nitrates and sulfates. The change in chemical content and properties of aerosols is coupled to change in particles' morphology. Furthermore, due to their different trajectories, dust storms result in different bacterial and fungal counts in particulate matter.

In this thesis, a comprehensive evaluation of the changes in bacterial and fungal content, morphology, sizes and chemical transformations of dust particles and their effect on the re-evaporation of acid gases and the deposition of aged and more soluble particles is offered. Results can be incorporated in regional models of aerosol transport, used for raising awareness related to health issues during dusty days and inform regulatory agencies on the changes and their impacts on the ecosystem during dusty episodes.

……..

CONTENTS

ILLUSTRATIONS

TABLES

CHAPTER I

INTRODUCTION

A. Particulate matter and dust storms

Particulate matter (PM) or aerosols are suspended particles (solids or liquids) released into the atmosphere by primary or secondary emission sources[1]. These particles are subject to many chemical and physical processes, depending on the meteorological and synoptic environmental conditions. Atmospheric aerosols are characterized by their elemental composition, mass concentration, size distribution, morphology, biological content, and most importantly by their diameter size[1]. Particles whose diameter is between 2.5 and 10 μm are commonly known as coarse particles, those whose diameter ranges between 2.5 and 0.25μm are particles in the accumulation mode, and those with diameters less than 0.25μ are ultrafine particles[2].

Coarse particles are produced by mechanical processes and are subject to long distance transport by convection and impaction, and to deposition by gravity or rainfall[3]. Sea-salts and mineral dust make a large fraction of coarse particles[4,5]. The smaller particles, on the other hand, are the result of chemical reactions and condensation processes (example

gas to particle conversions)[2,3,6]. These particles are resident in the atmosphere for days and weeks, unlike the coarse particles[2].

Dust outbreaks are known to alter the characteristics of local aerosols and result in changes in their physical and chemical states. The mixing of mineral dust with anthropogenic occurring aerosols[4,5], triggers the chemical and morphological deformation of primary atmospheric particles along with the formation of new secondary ones[7]. Beirut, being part of the northern hemisphere and lying on the eastern Mediterranean shore, is susceptible to two sources of dust storms: Arabian Desert and African Desert[8,9]. Dusty days are common during the spring and fall seasons[10], and have become more frequent in the region due to synoptic and climate changes[11-13]. A recent study, reviewing the past 49 years, reported a trend of 0.27 dusty days increase annually, along with elevated summer temperatures and longer periods of heat and droughts[14,15]. African dust storms originate from the Saharan Desert, which extends over North Africa, and are known to be the largest contributor to particulate matter in the atmosphere [13]. Such storms pass over highly populated urban areas (mainly Egypt), carrying along anthropogenic pollutants, and over the Mediterranean Sea carrying along marine aerosols[9,13,16,17]. Arabian Desert storms, originate in the Arabian Peninsula, and pass over an arid urban environment before reaching our region[7].

While few studies[18-23], conducted mainly at the American University of Beirut (AUB), characterize atmospheric particulate matter in Lebanon, this is the first study that defines the influence of dust-storms on the size segregated inorganic ion composition of

PM and the associated gases, the morphology of dust particles as well as the bioaerosols associated with dust.

B. Thesis Layout

Chapter II describes the influence of dust storms on mass concentration and inorganic ion content of the size segregated particulate matter in AUB, Beirut, Lebanon. The sampling was conducted on the roof top of the chemistry department at AUB. The dependency of PM composition on particle-size and Arabian dust outbreaks is explored. Results provide insights on the influence of aged mineral dust and marine aerosols mixed with anthropogenic pollution on the physical and chemical transformations taking place in the bulk of aerosols at the different sizes.

Chapter III outlines the correlations between acidic gaseous species and PM inorganic components collected during Arabian dusty and non-dusty days in AUB. In this chapter, we explore the mechanism of action relating gas-to-particle partitioning and its effect on the content of gases like HONO, HNO_3 and H_2SO_4 and nitrates and sulfates in particles.

Chapters IV and V describe the changes in the morphology as well as the bacterial and fungi counts associated with long-range transport of particles during dusty days.

Given the increase in the frequency of dust episodes in the Mediterranean region, this study offers a comprehensive evaluation of the changes in the bacterial and fungi content, morphology, sizes and chemical transformations of dust particles and their effect

on the re-evaporation of acid gases and the deposition of aged and more soluble particles. Results can be incorporated in regional models of aerosol transport, used for raising awareness related to health (increase of PM and bacterial count) during dusty days and inform regulatory agencies on the changes and their impacts on the ecosystem during dusty episodes.

CHAPTER II

INFLUENCE OF ARABIAN DUST TRANSPORT ON WATER-SOLUBLE INORGANIC IONS IN SIZE-SEGREGATED AEROSOLS IN BEIRUT

A. Introduction

Mineral dust appears as a large fraction of atmospheric aerosols, making up to 36% of the total [5,24], during normal days. These are particles with different sizes carried by short or long transport of air masses. The importance of studying such particles lies within their chemical composition and their pathogenic character. It has been known that these have light scattering and absorbing capabilities[8,25-28]. Also, studies have shown the capacity of dust particles to accommodate carcinogenic molecules, as well as, heavy metals; affecting the human health [29-31]. The smaller the particle diameter, the easier its access to the respiratory system and hence, the more it stimulates respiratory and cardiovascular diseases. This is when studying the composition of particles of different size diameters becomes necessary, and therefore relating all aforementioned characteristics to particle diameter.

Beirut, among other eastern Mediterranean cities, lies at the intersection of the three continents Asia, African and Europe and therefore experiences different trajectories of air masses carrying along particulate matter of different sizes and chemical components. First, Beirut experiences Northern winds coming from highly polluted and industrial Europe.

Also, it is subject to dust outbreaks originating in the Saharan desert in North Africa and passing over the Mediterranean Sea and Egypt [10]. Finally, East and South-east winds from the Arabian Desert pass over arid areas and Syria to our region [11-13]. Studies conducted in the north-western (Spain, France, Italy) [32-38] and eastern Mediterranean regions (Greece, Turkey, Israel) [20,23,39-51] emphasized the diversity of the atmosphere over the Mediterranean basin and the influence of dust events on aerosol composition.

In this study, size segregated aerosols are collected during Arabian dust outbreaks and compared to samples collected during non-dusty days, in terms of particulate mass distribution, ionic composition and ionic ratios. Also, acidic gas concentrations are determined. Results are also used to understand the effect of acidic gases on particle conversion and content, assess the aerosol chlorine depletion and neutralization factor of each size fraction, and to determine the effect of dust event on the nitrogen and sulfur solubility and deposition of particles onto the surface of the ocean.

B. Materials and Methods

1. Sampling location

Sampling was conducted around 40 m above sea level on the roof-top of the Chemistry department at the American University of Beirut; North-West Beirut, Lebanon. The site is surrounded by a green belt of trees and shrubbery from the South, and faces the Mediterranean Sea from the North. This sampling location is considered an urban background site which is affected mainly by sea breeze. Also, it is far from any industrial

pollution sources and the closest roadway is located around 150 m North-East. Further description of the site is detailed by Baalbaki et al. 2013 and Daher et al. 2013 [18,52] and its location is shown in Fig. 2.1.

2. HYbrid Single-Particle Lagrangian Integrated Trajectory (HYSPLIT)

48h air mass backward trajectories for all sampling days were checked using NOAA-HYSPLIT model [53,54] for the predication of dusty and non-dusty days. One model run per sampling day was considered for all sites, as sites are within few kilometers away from each other. HYSPLIT was run at three different altitudes between 1 and 5 km, the height of an average dust event. Samples were collected during Arabian dust outbreaks, which have low initial heights (2 to 4 km) and show east and south-east trajectories [7,55]. Dust days were confirmed using BSC Dream Atmospheric Dust Forecast System. Wind speed and direction, local weather and visibility were used as other indications to the occurrence of dusty days. Figure 2.1 displays the air mass trajectories of sampling days

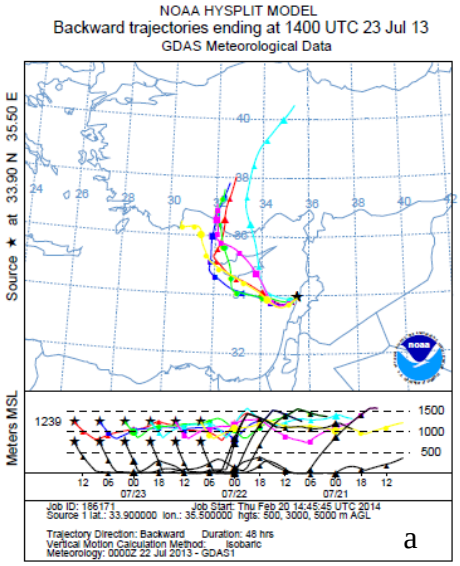
NOAA HYSPLIT MODEL
Backward trajectories ending at 1400 UTC 23 Jul 13
GDAS Meteorological Data
Source ★ at 33.90 N 35.50 E
Meters MSL
1239
1500
1000
500
07/23
07/22
07/21
Job ID: 186171 Job Start: Thu Feb 20 14:45:45 UTC 2014
Source 1 lat.: 33.900000 lon.: 35.500000 hgts: 500, 3000, 5000 m AGL
Trajectory Direction: Backward Duration: 48 hrs
Vertical Motion Calculation Method: Isobaric
Meteorology: 0000Z 22 Jul 2013 - GDAS1
a

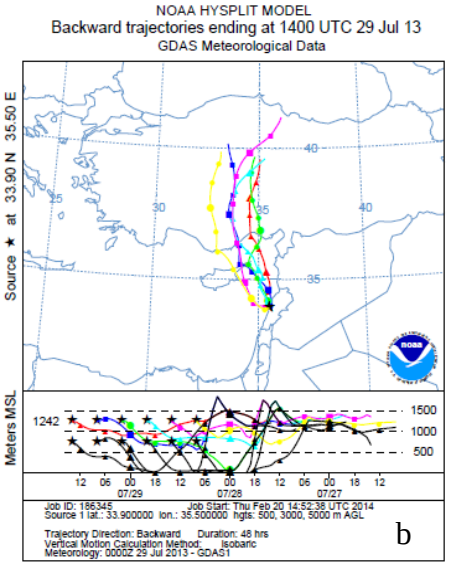
NOAA HYSPLIT MODEL
Backward trajectories ending at 1400 UTC 29 Jul 13
GDAS Meteorological Data
Source ★ at 33.90 N 35.50 E
Meters MSL
1242
1500
1000
500
07/29
07/28
07/27
Job ID: 186345 Job Start: Thu Feb 20 14:52:36 UTC 2014
Source 1 lat.: 33.900000 lon.: 35.500000 hgts: 500, 3000, 5000 m AGL
Trajectory Direction: Backward Duration: 48 hrs
Vertical Motion Calculation Method: Isobaric
Meteorology: 0000Z 29 Jul 2013 - GDAS1
b

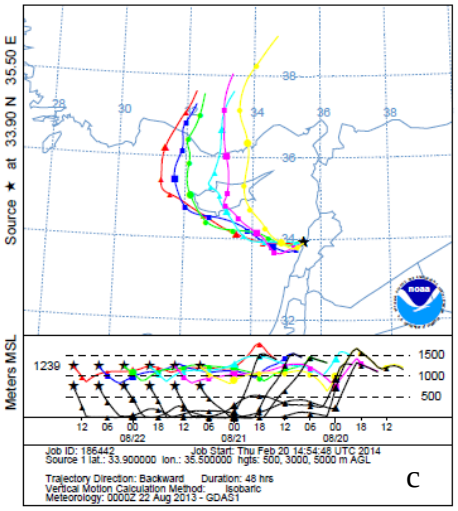
NOAA HYSPLIT MODEL
Backward trajectories ending at 1400 UTC 22 Aug 13
GDAS Meteorological Data
Source ★ at 33.90 N 35.50 E
Meters MSL
1239
1500
1000
500
08/22
08/21
08/20
Job ID: 186442 Job Start: Thu Feb 20 14:54:48 UTC 2014
Source 1 lat.: 33.900000 lon.: 35.500000 hgts: 500, 3000, 5000 m AGL
Trajectory Direction: Backward Duration: 48 hrs
Vertical Motion Calculation Method: Isobaric
Meteorology: 0000Z 22 Aug 2013 - GDAS1
c

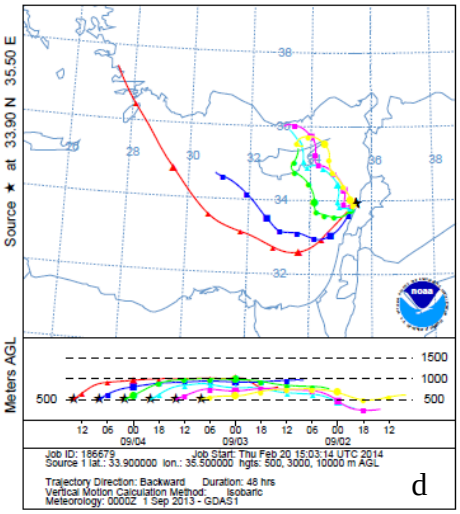
NOAA HYSPLIT MODEL
Backward trajectories ending at 1400 UTC 04 Sep 13
GDAS Meteorological Data
Source ★ at 33.90 N 35.50 E
Meters AGL
500
1500
1000
500
09/04
09/03
09/02
Job ID: 186679 Job Start: Thu Feb 20 15:03:14 UTC 2014
Source 1 lat.: 33.900000 lon.: 35.500000 hgts: 500, 3000, 10000 m AGL
Trajectory Direction: Backward Duration: 48 hrs
Vertical Motion Calculation Method: Isobaric
Meteorology: 0000Z 1 Sep 2013 - GDAS1
d

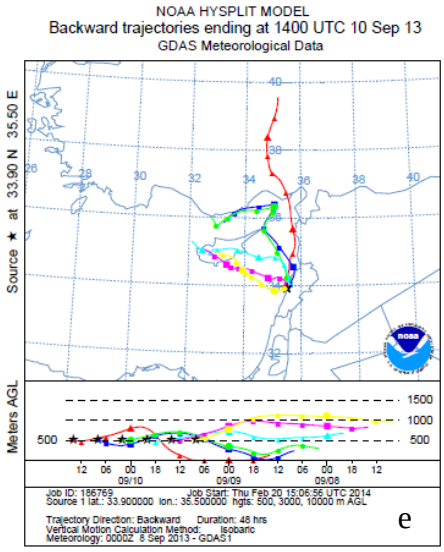
NOAA HYSPLIT MODEL
Backward trajectories ending at 1400 UTC 10 Sep 13
GDAS Meteorological Data
Source ★ at 33.90 N 35.50 E
Meters AGL
1500
1000
500
09/10
09/09
09/08
Job ID: 186769 Job Start: Thu Feb 20 15:06:56 UTC 2014
Source 1 lat.: 33.900000 lon.: 35.500000 hgts: 500, 3000, 10000 m AGL
Trajectory Direction: Backward Duration: 48 hrs
Vertical Motion Calculation Method: Isobaric
Meteorology: 00002 8 Sep 2013 - GDAS1
e

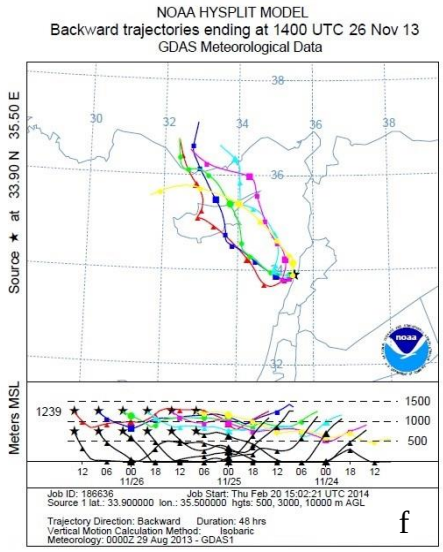
NOAA HYSPLIT MODEL
Backward trajectories ending at 1400 UTC 26 Nov 13
GDAS Meteorological Data
Source ★ at 33.90 N 35.50 E
Meters MSL
1239
1500
1000
500
11/26
11/25
11/24
Job ID: 186636 Job Start: Thu Feb 20 15:02:21 UTC 2014
Source 1 lat.: 33.900000 lon.: 35.500000 hgts: 500, 3000, 10000 m AGL
Trajectory Direction: Backward Duration: 48 hrs
Vertical Motion Calculation Method: Isobaric
Meteorology: 00002 29 Aug 2013 - GDAS1
f

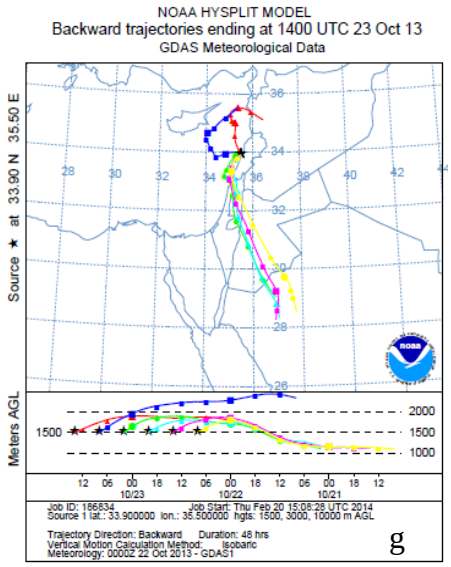
NOAA HYSPLIT MODEL
Backward trajectories ending at 1400 UTC 23 Oct 13
GDAS Meteorological Data
Source ★ at 33.90 N 35.50 E
Meters AGL
1500
2000
1500
1000
10/23
10/22
10/21
Job ID: 186634 Job Start: Thu Feb 20 15:08:26 UTC 2014
Source 1 lat.: 33.900000 lon.: 35.500000 hgts: 1500, 3000, 10000 m AGL
Trajectory Direction: Backward Duration: 48 hrs
Vertical Motion Calculation Method: Isobaric
Meteorology: 00002 22 Oct 2013 - GDAS1
g

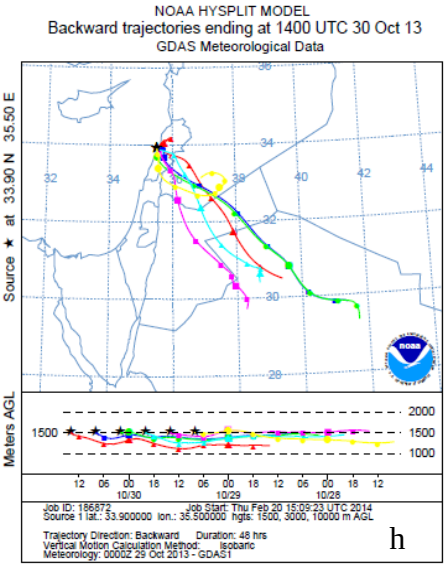
NOAA HYSPLIT MODEL
Backward trajectories ending at 1400 UTC 30 Oct 13
GDAS Meteorological Data
Source ★ at 33.90 N 35.50 E
Meters AGL
1500
2000
1500
1000
10/30
10/29
10/28
Job ID: 186872 Job Start: Thu Feb 20 15:09:23 UTC 2014
Source 1 lat.: 33.900000 lon.: 35.500000 hgts: 1500, 3000, 10000 m AGL
Trajectory Direction: Backward Duration: 48 hrs
Vertical Motion Calculation Method: Isobaric
Meteorology: 00002 29 Oct 2013 - GDAS1
h

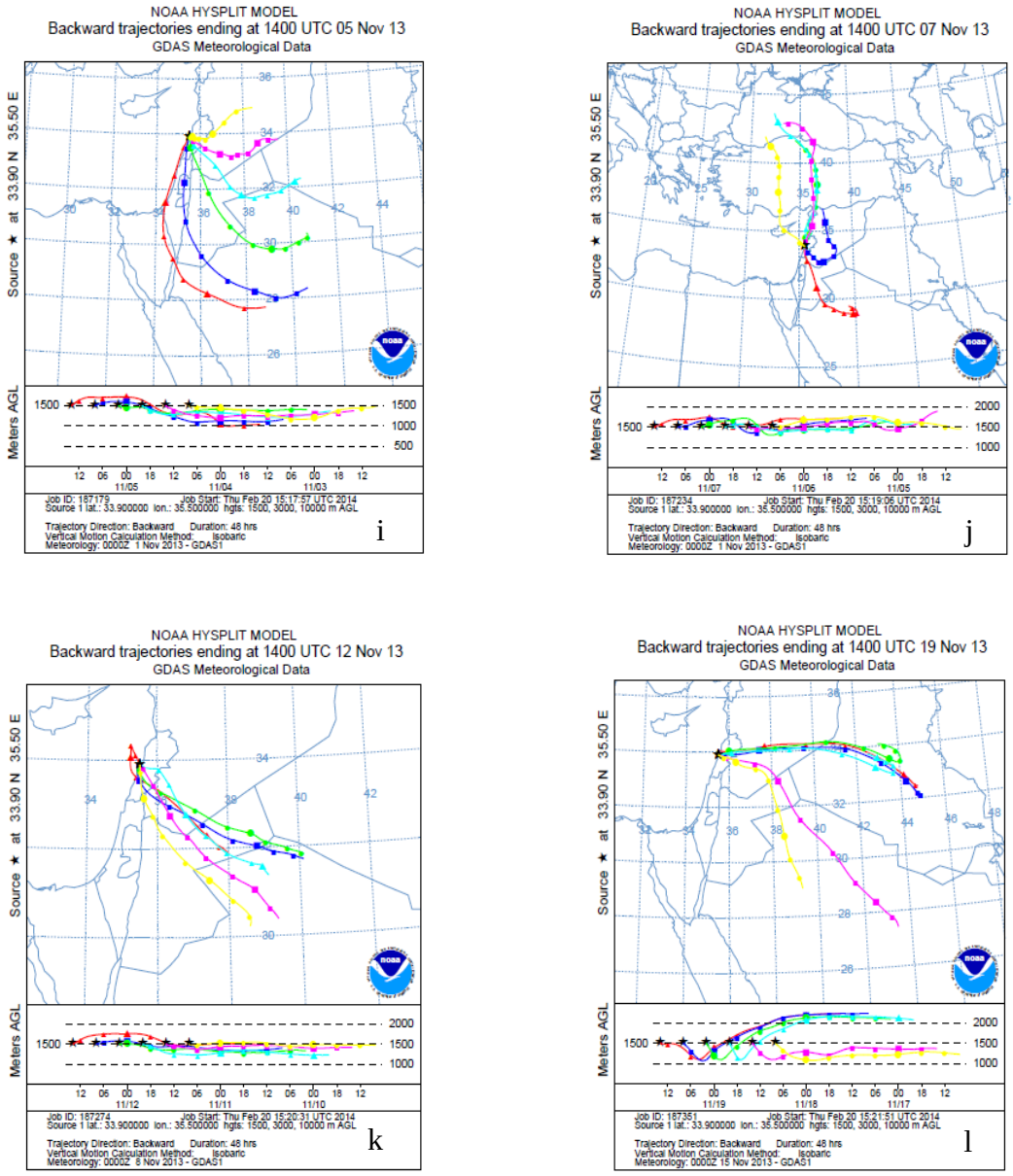

Figure 2.1 NOAA-HYSPLIT air mass trajectories showing: a-f) north and north west trajectories and g-l) east and south east trajectories.

3. Collection techniques

Soluble gases and size resolved aerosols were sampled between July and November 2013 at ambient level during dusty and non-dusty days. The aerosol and gas samples are collected using a Rupprecht & Patashnick Partisol 2300. Two sampling apparatus were set in parallel to account for %RSD. Following the sample procedure of Daher et al. 2013, aerosol collection extended over 24h using Sioutas Personal Cascade Impactor Samplers (Sioutas PCIS, SKC Inc., Eighty Four, PA, USA) preceded by PM_{10} inlets and operating at 9 l/min [52]. Dust particles were collected according to their size fractions; 10–2.5 μm (coarse) and 2.5–0.25 μm (accumulation) were collected on 25mm Teflon filters and <0.25 μm (quasi-ultrafine) were collected on 37 mm Teflon filters.

Soluble acidic gases (HONO, HNO_3 and H_2SO_4) were sampled for 24hr using a diffusion denuder system. The system is based on two Honey Comb denuders (HC) coated with 1% $NaCO_3$ and 1% glycerol in 50:50 water: methanol solution and placed in series in Rupprecht & Patashnick (R&P) Chemcomb™ cartridges. Sampling and analysis of trace gases is fully described in the following chapter and in Saliba and Chamseddine [22].

4. Gas Monitoring Station

The monitoring station is located at the roof top of the Chemistry department at the American University of Beirut (AUB). It is equipped with Thermo Environmental analyzers used to measure ozone (Model 49i, UV Photometric Prininciple), nitrogen oxides (Model 42i, Chemiluminescence Principle), sulfur dioxide (Model 43i, Pulsed Fluorescence

Principle), and carbon monoxide (Model 48i, Gas Filter Correlation infrared principle) (Table 2.1). The sampled air goes inside an inlet that is located 1 m above the station roof through glass and Teflon pipes and tubing. Mild heating and PTFE filters are used to retain condensed water molecules and particulate matter respectively from entering to the analyzers. The analyzers are calibrated using the Thermo Environmental Multigas Calibrator (Model 146i) for both zero and span concentrations. Zero air is provided from the Thermo Zero Air Generators (Model 111) connected to the Thermo Dual Reactor (Model 1150). Span gases are provided from standard gas bottles for NO, CO and SO_2. O_3 was internally generated inside the calibrator.

The Met One instruments (http://www.metone.com/meteorology.php) were used to setup the weather station that records wind speed and direction, air temperature, relative humidity, pressure, solar radiation and precipitation at a logging interval of 1 min. It is placed on a pole that was lifted about 5 m above the monitoring station at the AUB-Chemistry roof top.

Table 2.1 General specifications for the Thermo Environmental gas analyzers

	Logging time	**Flow rate (L/min)**	**Detection limit (ppb)**	**Precision (ppb)**
NO_x	1 min	0.6	0.4	± 0.4
SO_2	1 min	0.5	<0.5	± 1

5. Ion Chromatography

Coated denuders are extracted by a 20mL of Deionized water for the detection of soluble acidic gases. Each Teflon was placed in a 25ml sterile conical flask with 20 ml of deionized water and sonicated for 50 min for the removal of of anions (Br^-, F^-, Cl^-, NO_2^-, NO_3^-, and SO_4^{2-}) and cations (Na^+, NH_4^+, K^+, Mg^{2+}, and Ca^{2+}).

Both extracts are micro-filtered and analyzed by ion chromatography [22] then analyzed using ion chromatography Metrohm 850 professional IC AnCat with 858 Professional Sample Processor.

Cation separation was accomplished using a METROSEP C4 -150/4.0 IC analytical column (4.0 ×150.0 mm) with a 10-µl sample loop. The cation mobile phase is 2.5 mM Nitric acid (prepared by dissolving 0.310 ml of 65% nitric acid in 2L of 18.2 mΩ Ultrapure water at a flow rate of 0.9 ml/min at 25℃.

Anion separation was accomplished using a METROSEP A Supp 7 -250 (4.0mmID ×250mmL) analytical column with a 50-µl sample loop. A solution of 3.6 mM Na_2CO_3 was used as an eluent at a flow rate of 0.8 ml/min at 45℃.

a. Calibration and standardization

The calibration curves of each anion and cation are reported in Table 2.2

Table 2.2: Calibration Curves of cations and anions and their corresponding correlation coefficients

Date		Na^+	NH_4^+	K^+	Mg^{2+}	Ca^{2+}
23/01/2014	**Equation**	y = 0.1565x	y = 0.0195x + 0.0051	y = 0.0905x	y = 0.3448x	y = 0.1966x
	R^2	0.9998	0.999	0.9996	0.9988	0.9995
30/01/2014	**Equation**	y = 0.1659x	y = 0.2272x	y = 0.0973x	y = 0.3469x	y = 0.1983x
	R^2	0.9997	0.9997	0.9995	0.9998	0.9999
Date		Cl^-	NO_2^-	NO_3^-	PO_4^{3-}	SO_4^{2-}
23/08/2013	**Equation**	y = 0.3015x - 0.0427	y = 0.2089x - 0.0342	y = 0.1472x - 0.0145	y = 0.1964x - 0.0228	y = 0.0705x - 0.006
	R^2	0.9989	0.9989	0.9987	0.9983	0.9991
30/10/2013	**Equation**	y = 0.3063x - 0.0624	y = 0.2122x - 0.0479	y = 0.1505x - 0.0282	y = 0.0717x - 0.0109	y = 0.2014x - 0.0431
	R^2	0.9998	0.9998	0.9998	0.9997	0.9997
8/12/2013	**Equation**	y = 0.3009x - 0.0404	y = 0.2093x - 0.0272	y = 0.1471x - 0.0181	y = 0.0701x - 0.0063	y = 0.1967x - 0.0271
	R^2	0.9991	0.9991	0.9991	0.9994	0.9991
15/1/2014	**Equation**	y = 0.128x - 0.0558		y = 0.0888x - 0.0385	y = 0.0616x - 0.0249	y = 0.0291x - 0.0141
	R^2	0.9995		0.9992	0.999	0.999
11/2/2014	**Equation**	y = 0.2815x - 0.0344		y = 0.1378x - 0.021	y = 0.064x - 0.0091	y = 0.1788x - 0.0198
	R^2	0.9991		0.9991	0.9992	0.9993

b. LOD and LOQ

LOD defined as the limit of detection of the ion chromatography machine, is the concentration of a certain element that the Ion chromatography machine is able to detect.

It is calculated by going as low as possible in concentration, running the same concentration 3 times, and computing the standard deviation of these. Followed by drawing a linear calibration curve, the slope is used in the following formula:

$$\text{LOD} = 3\frac{s}{m}$$

where s in the standard deviation and m is the slope. LOD for the cations was found to be: 0.0055, 0.0021, 0.087, 0.0036, 0.012, and 0.038 for Na^+, NH_4^+, K^+, Mg^{2+}, and Ca^{2+} respectively. For the anions the LOD was found to be 0.0016, 0.0002, 0.0069, 0.015 and 0.0026 for Cl^-, NO_2^-, NO_3^-, PO_4^{3-} and SO_4^{2-} respectively.

LOQ is the limit of quantification of the Ion chromatograph. It is calculated by following the same procedure above, however using the following formula:

$$\text{LOQ} = 10\frac{s}{m} \quad ;$$

where s is the standard deviation and m is the slope. LOQ for the cations was found to be: 0.0069, 0.29, 0.011, 0.039 and 0.13 for Na^+, NH_4^+, K^+, Mg^{2+}, and Ca^{2+} respectively. For the anions the LOD was found to be 0.007, 0.02, 0.012, 0.039, and 0.13 for Cl^-, NO_2^-, NO_3^-, PO_4^{3-} and SO_4^{2-} respectively.

c. Blank

i. Blank denuders

Coated denuders are kept in a purged glove box during the sampling time, and later extracted and analyzed via IC to serve as a background. Prior to each sample run, deionized water alone and the coating solution is analyzed via IC to account for any contamination. To eliminate any cross contamination between samples, six denuders are labeled by numbers 1D-6D, placed in beakers labeled 1B-6B, filled with deionized water and sonicated. The water is removed, then the beakers are refilled and the denuders are sonicated again. During each sample collection, the denuders used in each cartridge are identified and thereby the corresponding blank denuder is used as a background reference.

ii. Blank Filters:

To account for the ions present in blank filters, three Teflon filters of each diameter size (33mm and 25mm) were extracted in 20ml deionized water by 50 minutes of sonication at 80MHz following the same extraction procedure of the sampled filters. The extracts were filtered using 0.25µm syringe filters and analyzed by IC. The average areas of the blanks were subtracted from the sampled filters' areas for each filter size.

C. Results and discussion

1. Characteristics of Dust Storms

Beirut experiences three different types of air trajectories [10]. First, north and north-west winds, originating from Europe and passing over the Mediterranean Sea, are identified as non-dusty days (Fig. 2.1 a-f). West and south west trajectories, on the other hand, originate from the Saharan Desert which extends over North Africa, pass over Egypt and are known as African Dust Storms. These are mostly frequent during the Spring season and usually last between 2 to 4 days[13]. Finally, air masses showing east and south-east trajectories are known as Arabian Desert storms. These originate from the Arabian Peninsula, pass over Syria and usually occur in the Fall Season for a duration that lasts for 1 day [16]. Since, in this study the sampling campaign is conducted during the Fall Season of year 2014, the dust-storm samples collected are identified by HYSPLIT to have east and south-east wind trajectories (Fig. 2.1 g-l) and are, therefore, of an Arabian origin.

2. Coarse, accumulation and fine mass concentration of particulate matter

The mass distribution of PM according to diameter size is shown in Table 2.3. During non-dusty days average Total PM was found to be 48.72μg/m^3 in comparison to dusty days where the average almost doubles to reach 92.81μg/m^3. During dust outbreaks, Total PM concentration reached a maximum of 135.92μg/m^3 accompanied with an increase of temperature and decreased visibility. Although this increase in total PM concentration is attributed to an increase in all size fractions of dust, the accumulation fraction showed the

highest increase (208%), followed by the coarse (117%) and fine (4.6%) fractions, respectively.

Table 2.3: Size-resolved mass concentrations of particulate matter (PM) during non-dusty and dusty samples

Non-Dusty	UF (µg/m³)	Acc (µg/m³)	CPM (µg/m³)	Total PM
23-Jul-13	26.33	15.46	25.59	**67.38**
29-Jul-13	12.97	6.58	14.85	**34.4**
22-Aug-13	17.94	7.32	15.50	**40.76**
4-Sep-13	13.79	5.94	23.99	**43.72**
10-Sep-13	22.26	6.34	22.44	**51.03**
26-Nov-13	19.30	11.11	24.64	**55.05**
Dusty	**UF (µg/m³)**	**Acc (µg/m³)**	**CPM (µg/m³)**	**Total PM**
23-Oct-13	21.64	10.39	29.10	**61.14**
30-Oct-13	16.46	22.44	53.22	**92.12**
5-Nov-13	19.78	38.44	63.41	**121.63**
7-Nov-13	18.99	42.44	74.52	**135.95**
12-Nov-13	16.71	33.59	36.58	**86.88**
19-Nov-13	24.24	15.22	18.97	**58.43**

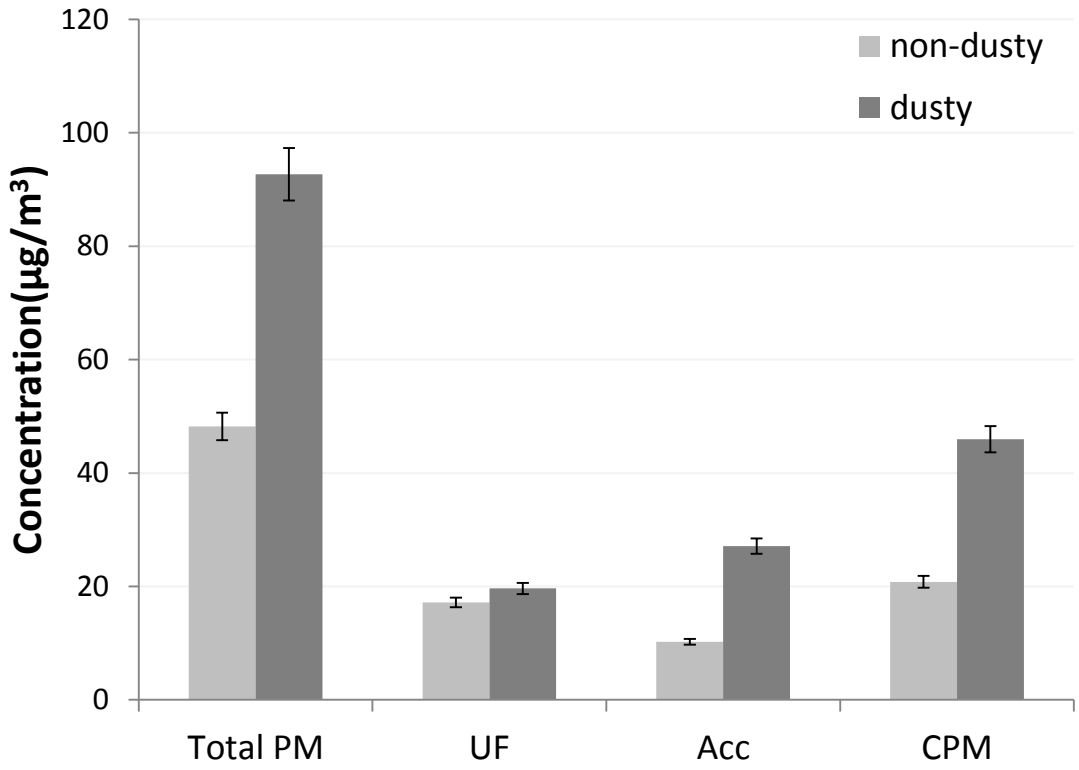

Figure 2.2: Bar graph showing the concentrations of total PM and each size fraction during non-dusty and dusty days (UF: Ultrafine, Acc: accumulation , CPM: coarse particulate matter)

3. Sea Salts (SS)

SS contribution was estimated as the sum of Na^+ concentration and sea-salt fractions of Cl^-, Mg^{2+}, K^+, Ca^{2+}, and SO_4^{2-} concentrations, assuming standard sea-water composition using soluble Na^+ as a tracer for sea-salt [6,56]; and where

$[Na^+]_{ss} = [Na^+]_{total}$

$[Cl^-]_{ss} = 1.8\ [Na^+]$

$[Mg^{2+}]_{ss} = 0.12[Na^+]$

$[K^+]_{ss} = 0.036[Na^+]$

$[Ca^{2+}]_{ss} = 0.038[Na^+]$

$[SO_4^{2-}]_{ss} = 0.252[Na^+]$

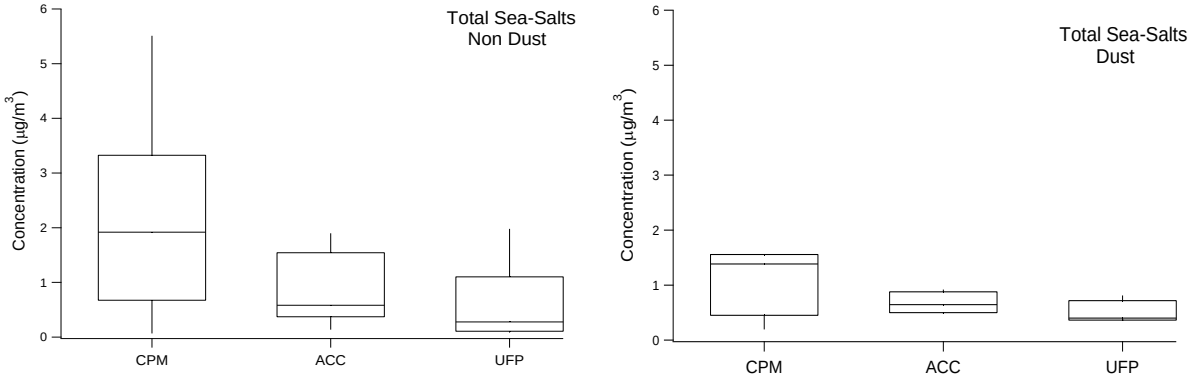

Figure 2.3: Box plots showing the sea-salt ions in CPM, ACC and UFP fractions during non-dusty and dusty days (Lowest whiskers represent the lowest concentration, the highest whiskers represent the highest concentration, the middle represents the average).

The coarse mode makes the largest contribution to sea-salts. This is in line with sea-salt aerosol distribution (Seinfield Figure 7.23 page 441)[6], followed by the accumulation

and the fine as shown in Figure 2.3. In dusty days, the decrease in the overall concentration of all sea-salts in all size fractions is seen during dusty days (Fig. 2.3); average sea-salts' concentration in the coarse mode decreases from 2.15 to 1.13 $\mu g/m^3$, in the accumulation mode from 0.85 to 0.76 $\mu g/m^3$ and in the ultrafine fraction from 0.59 to 0.55 $\mu g/m^3$. This is due to air-mass trajectories originating from arid lands and competing with local sea-breeze.

Ionic chloride to sodium ratio

Also, the ionic ratio of Cl^-/Na^+ has been studied for all size fractions during dusty and non-dusty. The typical sea-salt ratio is 1.81 [57,58]. Since sea-salts are mainly concentrated in the coarse size fraction [6,59], the focus of chloride depletion assessment in this section will be on this size fraction. It is found that the Cl^-/Na^+ ratio drops from 1.41 during non-dusty days to 0.93 during dusty days. These results are consistent with data from previous years, in which, for most sampling days chlorine depletion is attributed to several reactions that take place in the atmosphere in the presence of acid gases as shown in reactions (1)-(8) [57,59-70]:

$$HNO_{3\,(g)} + NaCl_{\,(s,\,aq)} \rightarrow NaNO_{3\,(s,\,aq)} + HCl_{\,(g)} \quad (1)$$

$$H_2SO_{4\,(aq)} + 2NaCl_{\,(s,\,aq)} \rightarrow Na_2SO_{4\,(s,\,aq)} + 2HCl_{\,(g)} \quad (2)$$

$$2NO_{2\,(g)} + NaCl_{\,(s,\,aq)} \rightarrow ClNO_{\,(g)} + NaNO_{3\,(s,\,aq)} \quad (3)$$

$$N_2O_{5\,(g)} + NaCl_{\,(s,\,aq)} \rightarrow ClNO_{2\,(g)} + NaNO_{3\,(s,\,aq)} \quad (4)$$

$ClONO_{2\,(g)} + NaCl_{\,(s,\,aq)} \rightarrow Cl_{2\,(g)} + NaNO_{3\,(s,\,aq)}$ (5)

$ClNO_{2\,(g)} + h\nu \rightarrow Cl + NO_{2(g)}$ (6)

$Cl_{2(g)} + h\nu \rightarrow 2Cl.$ (7)

$Cl. + O_3 \rightarrow ClO. + O_2$ (8)

Hence, chorine depletion identified by such heterogeneous replacement of Cl^- occurs and therefore results in the formation of particulate NO_3^- and SO_4^{2-} and the release of HCl in the atmosphere via reactions (1) and (2). Furthermore, reactions (4)-(8) lead to the formation of $ClNO_{2(g)}$ and $ClNO_{(g)}$ which upon photolysis generate Cl· radical. This latter has been shown to be important able to act as a source or a sink of ozone depending on the levels of NO_x and Hydrocarbons in the troposphere[71,72].

4. Crustal ions

Non sea-salt Potassium, Magnesium and Calcium, are considered crustal elements [56]. They experience 65, 60 and 75% increase, respectively, during dusty days. During non-dusty, Mg is more abundant in the accumulation and fine fractions (Fig. 2.4), and is identified to be emitted from primary sources [73] . Ca (Fig. 2.5) appears in the coarse mode during non-dusty days indicating that it originates from sources different than those of magnesium, and are attributed mainly to dust resuspentions [74]. During dusty days Ca^{2+} and Mg^{2+} exhibit similar trends of variation with the coarse fraction being affected the most (81% increase in the coarse vs 76% and 61% in the accumulation and ultrafine, for calcium

and 172% increase in the coarse vs 43% and 5% in the accumulation and ultrafine, respectively for magnesium). This can be attributed to soil-derived Mg and Ca enriching the air parcels originating from the Arabian Desert [8].

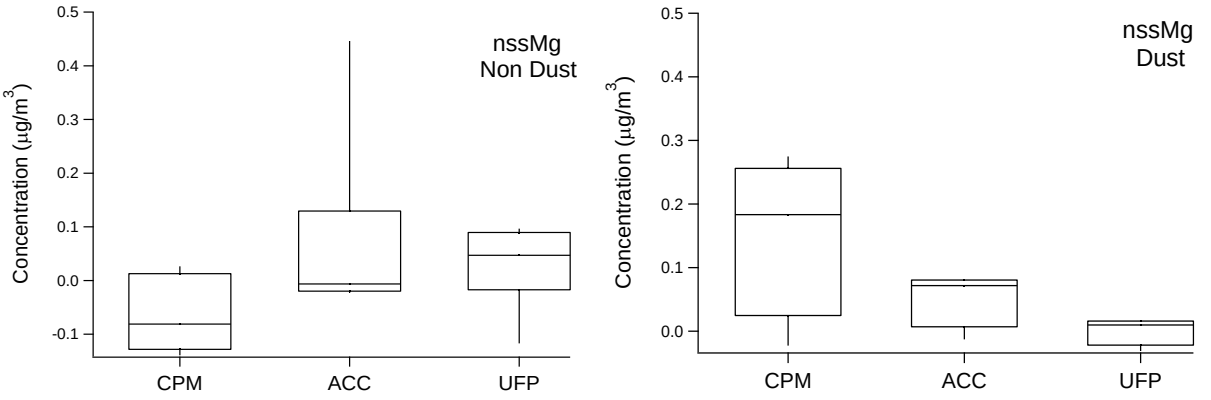

Figure 2.4: Box plots showing the non-seasalt magnesium ions in CPM, ACC and UFP fractions during non-dusty and dusty days

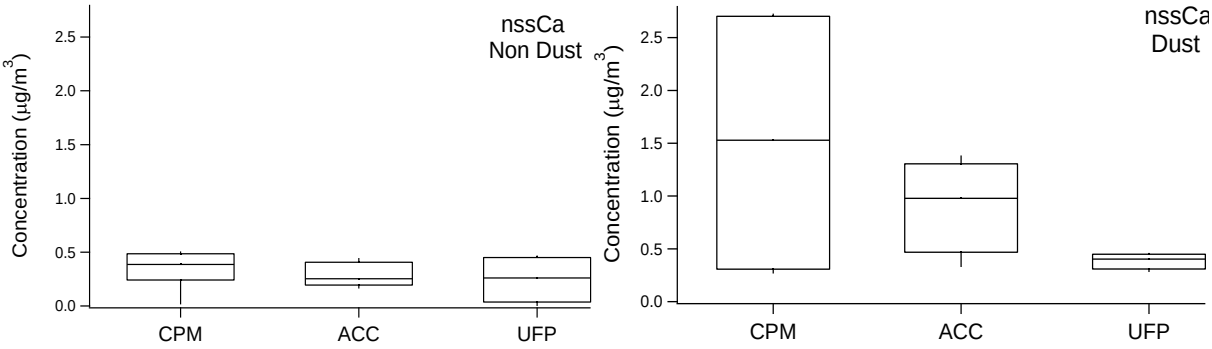

Figure 2.5 Box plots showing the non-seasalt Calcium ions in CPM, ACC and UFP fractions during non-dusty and dusty days

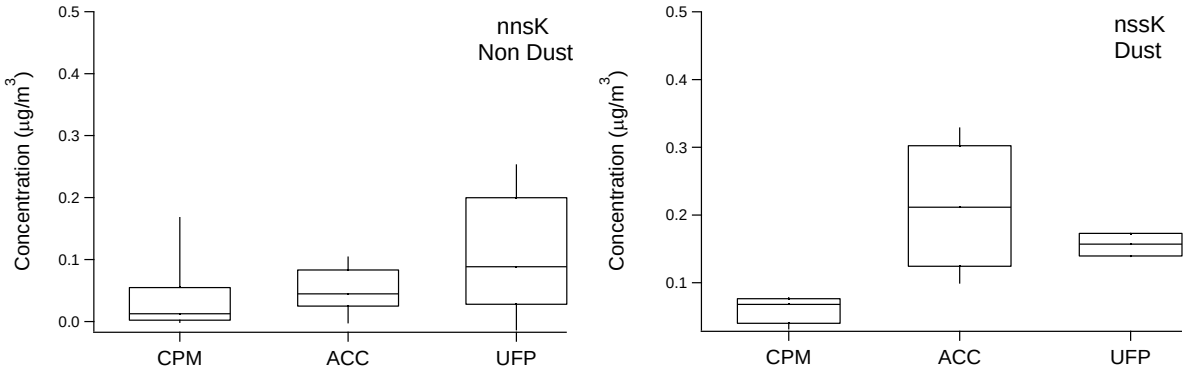

Figure 2.6: Box plots showing potassium ion concentrations in CPM, ACC and UFP fractions during non-dusty and dusty days

Average K^+ (Fig.2.6) shows a 77% increase in the accumulation mode in comparison to 54% increase in the coarse. K^+ in the accumulation mode originates from biomass burning and agricultural activities [75,76]. Blowing dust is another source of potassium [77]. Furthermore, KNO_3 is known to be a component of propellants and explosives [78] and could have been carried from Syrian Civil war to our sampling location during dusty days [7]. In fact, crystals rich with KNO_3 were imaged by SEM during dusty events and are reported by our group [7]

5. Nitrates and Sulfates

While fresh mineral dust particles in the troposphere are inert, aged by soluble aerosol components, these mineral particles will have altered sizes and shapes in addition to becoming more hygroscopic; rendering, thereby, the aerosols more efficient as Cloud Condensation Nuclei (CCN) [8,79-81]. Therefore, knowledge about the soluble components

coating or reacting with mineral particles is important. Of these reactions are the enhanced reactions of mineral dust with urban acidic gases which lead to the transformation of mineral dust particles into sulfates and nitrates enriched particles.

During non-dusty days, nitrates are more concentrated in coarse fractions, followed by accumulation and fine fraction (Fig. 2.7) and are consistent with measured size distribution of urban nitrate aerosols discussed by Seinfield and Pandis and references therein [6,59]. Nitrates follow the same size distribution trend during dusty days, yet experience a huge increase by 73, 74 and 58% in the coarse, accumulation and fine fractions, respectively. This result is in agreement with previous analyses done in Beirut [22]. Several possible mechanisms contribute to the formation of nitrates in particulate matter as illustrated in reactions (1), (3), (4), (5) and (9) [82]. Reaction (9) is a heterogeneous reaction that takes place only at higher relative humidity. Other homogenous and heterogeneous reactions could involve the interaction of HNO_3 with $Ca(CO_3)_2$, $Mg(CO_3)_2$ and KCl to form $Ca(NO_3)_2$, $Mg(NO_3)_2$, and KNO_3(Reactions (10)-(12)) [83,84]. This mechanism is supported by the increase of crustal elements during dust and by the correlations between crustal elements and nitrates during these dusty days, which appear to be the highest in the coarse particles mode. The correlations in the coarse appear as $r^2 = 0.91$ between K^+ and NO_3^-, $r^2 = 0.65$ between Na^+ and NO_3^- , $r^2 = 0.99$ between Ca^{2+} and NO_3^- and finally $r^2 = 0.28$ between Mg^{2+} and NO_3^-.

$$2NO_{2(g)} + H_2O \rightarrow HONO_{(g)} + HNO_{3(p)} \qquad (9)$$

$$Ca(CO_3)_2 + 2HNO_3 \rightarrow Ca(NO_3)_2 + 2H^+_{(aq)} + 2CO_3^{2-}{}_{(aq)} \qquad (10)$$

$$Mg(CO_3)_2 + 2HNO_3 \rightarrow Mg(NO_3)_2 + 2H^+_{(aq)} + 2CO_3^{2-}{}_{(aq)} \quad (11)$$

$$KCl + HNO_3 \rightarrow KNO_3 + HCl_{(g)} \quad (12)$$

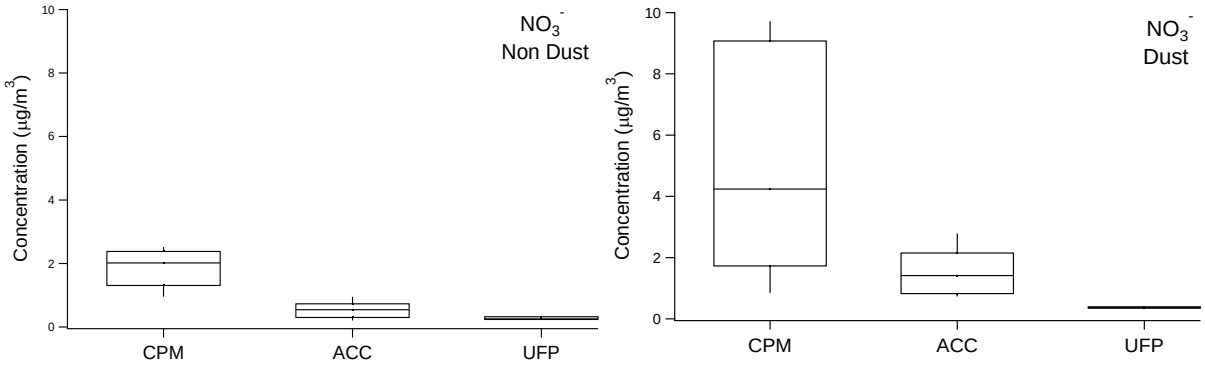

Figure 2.7: Box plots showing the nitrate ion concentrations in CPM, ACC and UFP fractions during non-dusty and dusty days

In Fig. 2.8, it is shown that sulfates in the particulate phase are more abundant in the ultrafine fraction, followed by the accumulation, then the coarse mode during non-dusty days. In urban aerosol distribution studies, sulfate is shown to have a peak concentration at 0.2 µm diameter corresponding to the condensation mode [59,85]. Sulfates experience an increase in the total concentration during dusty days which is mainly emphasized by 79% and 60% increase in the accumulation and fine size fractions, respectively. This phenomenon is in agreement with previous studies which show that sulfates during dusty days are mainly concentrated in particles less than 2.5µm in diameter [19,56]. Sulfates in the fine mode is attributed to the nucleation of which gas into $(NH_4)_2SO_4$ [6,86]. This is confirmed by the correlation between NH_4^+ and SO_4^{2-} in the accumulation fraction ($r^2 = 0.98$) and ultrafine fraction ($r^2 \sim 1$). Sulfates, in all size fractions, are also carried by blown wind, as $CaSO_4$ from crustal origin, (Reaction (13) [7,87]) or from the reaction of H_2SO_4 with sea salts,

(Reaction (14) [6,57,88]). Considering all these reactions, SO_4^{2-} is expected to associate with H^+ rather than crustal elements (coarse)[89] and its production from sea-salts (coarse) is limited [90]. Sulfate formation as a result of nucleation with emitted ammonia gas (fine) is mostly favored [6]; hence, the abundance of sulfates in the accumulation and ultrafine size fractions.

$$CaCO_{3(p)} + H_2SO_4 \rightarrow CaSO_{4(p)} + 2H^+_{(aq)} + CO_3^{2-}{}_{(aq)} \quad (13)$$

$$2NaCl_{(p)} + + H_2SO_4 \rightarrow Na_2SO_{4\,(p)} + 2HCl_{(g)} \quad (14)$$

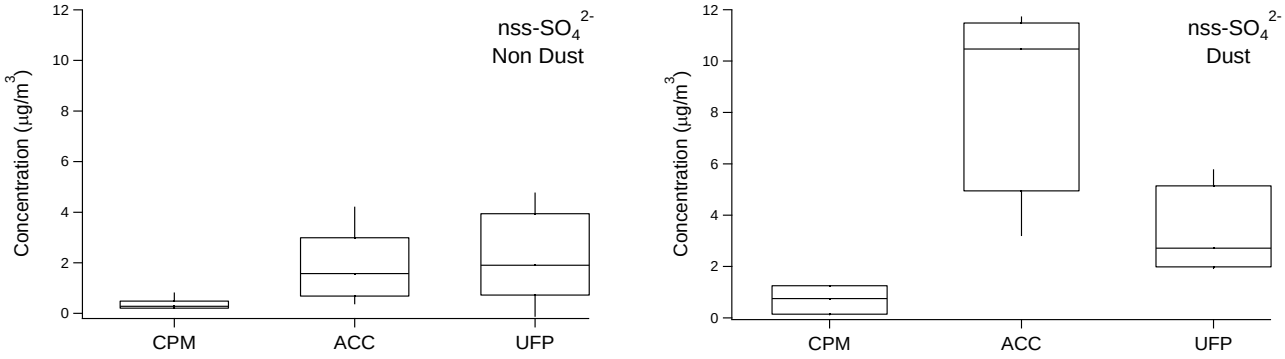

Figure 2.8 Box plots showing the non-seasalt sulfate ion concentrations in CPM, ACC and UFP fractions during non-dusty and dusty days

6. Other ions

Ammonia readily reacts with sulfuric acid (H_2SO_4) to form non-volatile aerosol species like the fully neutralized ammonium sulfate [$(NH_4)_2SO_4$] [91]. Additional NH_3 can react with HNO_3 and other acidic gases to form semi-volatile salts. Ammonium nitrate (NH_4NO_3) residence time in the particle phase strongly depends on temperature and relative humidity, where colder, more humid conditions will shift the equilibrium to the particle phase [92]. Ammonia is thus an important precursor to particulate matter in the accumulation and ultrafine modes (< $PM_{2.5}$) which has a longer atmospheric lifetime than gaseous NH_3 and can therefore be transported and deposited further downwind [93,94]. Such transport has

an important effect on nitrogen-deposition and consequently affecting the soil acidification, and biodiversity loss in sensitive ecosystems [95-98].

Ammonium concentration, during non-dusty days, is the highest in the ultrafine fraction as shown in Fig.2.9, followed by the accumulation then the coarse, and is consistent with several studies that identified ammonium to exist in the fine mode [89,99]. Ammonium experiences a 78% increase in its total mass concentration when going from non-dusty to dusty days. This increase is seen mostly in the accumulation mode with a concentration of 2.2 $\mu g/m^3$; corresponding to around 92% increase. In fact, secondary ammonium aerosols have been shown to have a peak concentration at around 0.2 μm, concentrated most in the condensation mode [85]. Ammonium is mostly correlated with sulfates and nitrates (Table 2.4) via reactions (15) and (16)[6]. Emitted ammonia, originates from soil, animal waste, fertilizers, agricultural activities and other man-made practices [91,100].

$$NH_{3(g)} + HNO_3 \rightarrow NH_4NO_{3(s)} \quad (15)$$

$$NH_{3(g)} + H_2SO_4 \rightarrow (NH_4)_2SO_{4(s)} \quad (16)$$

In this study, the aerosol medium characterization as ammonium rich or poor is considered. Ammonium richness is defined by the molar ratio of $[NH_4^+]/[SO_4^{2-}]$. A medium is known to be ammonium rich if this ratio is greater than 1.5 [101]. During non-dusty days, the highest ratio appeared for the coarse particles (1.1) followed by the ultrafine (0.5) explained by the occurrence of lower percentage of sulfates in these two size fractions[6,59]. For the accumulation mode, where the ammonium concentration is minimal

(Fig 2.9), the ratio is 0.3; thus all three fractions define an ammonium poor medium, as expected[22]. During dusty days, ammonium to sulfate ratio (0.7) presents a higher value than the non-dusty ultrafine ratio (0.5) and is explained by the huge increase of accumulation phase NH_4^+, presented earlier (Fig 2.9). Also, the coarse particles did not display a major change in the ammonium to sulfate ratio and shows an ammonium poor medium as well.

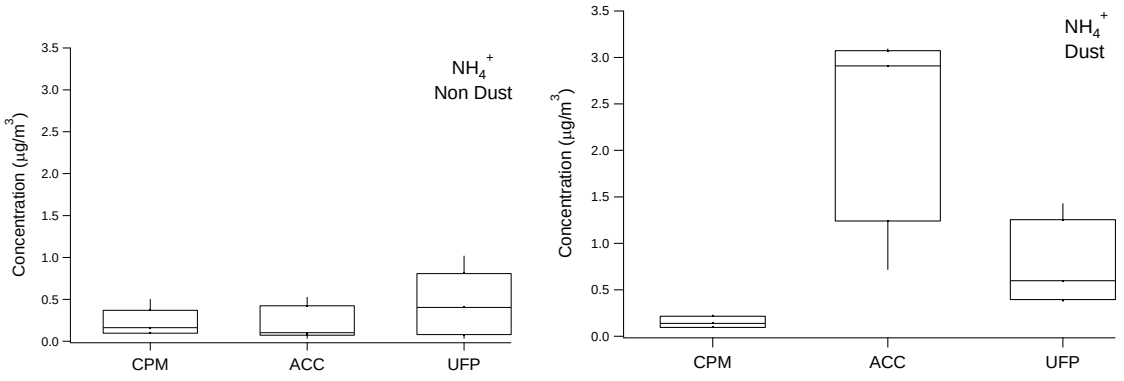

Figure 2.9: Box plots showing the ammonium ion concentrations in CPM, ACC and UFP fractions during non-dusty and dusty days.

Table 2.4: Correlation coefficients (r^2) for ammonium with nitrates and sulfates in different (PM) size fractions collected during non-dusty and dusty days in the 2013 field campaign

		Non-Dusty			Dusty			
		Ammonium						
		UF	Acc	CPM		UF	Acc	CPM
Sulfate	UF	0.92			UF	**1.00**		
	Acc		0.03		Acc		**0.98**	
	CPM			0.01	CPM			0.65
Nitrate	UF	0.19			UF	0.09		
	Acc		0.01		Acc		**0.77**	
	CPM			0.20	CPM			**0.71**

Ammonium concentration is directly related to the degree of neutralization of acidity of aerosols and the neutralization factor; calculated by [102]:

$$NR = \frac{[NH_4^+]}{[SO_4^-]_{nss}+[NO_3^-]};$$

where NR is the neutralization factor, $[NH_4^+]$ and $[NO_3^-]$ are the particulate phase molar concentration of ammonia and nitrate, respectively, and $[SO_4^{2-}]_{nss}$ is non-seasalt sulfate calculated by $[SO_4^{2-}]_{nss}=[SO_4^{2-}]_{total} - [SO_4^{2-}]_{ss}$ (explained in "Seasalts" section). The neutralization factor calculated for each size fraction of PM for dusty and non-dusty days is shown in Table 2.5. All the calculated ratios were below 1 which confirms as shown earlier that ammonium is not efficient in neutralizing the acidity of aerosols [101,103]. Other cations such as K^+, Na^+, Ca^{2+} and Mg^{2+} are responsible for the removal of acidic sulfates and nitrates from PM. Our results are in agreement with previous studies that show that our region is deficient in ammonium [22,104,105].

In fact, aerosol acidity, H^+ molar concentration, is calculated using the difference between molar equivalents of anions and cations [106-108] with negative value signifies the absence of acidity per aerosol [109].

$$[H+] = [Anions] – [Cations]$$

While no excess acids are determined in non-dusty days, aerosols' acidity is found to be higher in dusty days. The effect of such difference in the acidity of the aerosol on the evaporation of acidic gases like HCl, HNO_3 and H_2SO_4 will be discussed in the next chapter.

Table 2.5: Acidity and neutralization factor of aerosols during non-dusty and dusty days

	Total [H^+] (mol/m^3)			NR (mol/m^3)		
	UF	**Acc**	**CPM**	**UF**	**Acc**	**CPM**
Non Dust	0.0004	0.0019	-0.0089	0.3517	0.2864	0.5381
Dust	0.0069	0.0211	-0.0072	0.5548	0.6144	0.2640

7. Acidic gases species

Acidic gases analyses during dusty and non-dusty days are present in Table 2.6. In this study, HCl is found to be more abundant during non-dusty days, where its concentration is 1.56 and 0.8 μg/m^3, respectively. This 0.77 μg/m^3 decrease is in agreement with its precursors, where particulate Cl^- decrease during similar days. HCl originates from sea-salt reactions with $HNO_{3\,(g)}$ and $H_2SO_{4\,(g)}$ reactions (1), (2), (12) and (14) [56] through chlorine depletion phenomena, discussed earlier. This mechanism is important during days with high relative humidity (non-dusty days in this study), in which acidic gases are not engaged with other deposition processes. During Arabian dust-outbreaks, the average relative humidity drops, the chlorine replacement becomes less significant and therefore results in a decrease in released HCl. Also, HCl shows some anthropogenic sources associated with coal-burning, domestic waste burning and waste incineration [110].

HONO gas, which is an important precursor for OH radicals in the atmosphere [1] increased by three-folds during Arabian dust days reaching a maximum of 3.5μg/m^3 (Fig 2.10). The HONO correlation with NO_2 and its relation with particulate phase nitrate will be discussed further in the following chapter.

Similarly, HNO_3 experiences an increase during dusty days. HNO_3 is involved in reactions leading to chlorine depletion and nitrate formation. HNO_3 is formed mainly from the oxidation of NO_2 by OH^-. NO_2, which also increases during dusty episodes (Fig. 2.10), is formed from the oxidation of anthropogenic NO and by tropospheric ozone or light (hν) [111-113]. Moreover, HNO_3 is the major species involved in atmospheric dry and wet deposition in the nitrogen cycle. It is lost by dry deposition on land or by wet removal, also known as wet deposition. Another mechanism for the removal of nitric acid is its reaction with ammonia gas to form NH_4NO_3, which is very volatile and results in a major exchange between gas and solid phases [114] and results in daily variations of HNO_3 level depending on temperature and relative humidity [92].

Finally, SO_2 and its oxidized form, H_2SO_4 show a huge increase during dust storms attributed mainly to anthropogenic emission [115], especially industrial emissions [116], that have undergone long range transport. Other sources of SO_2, which also increases during dusty days, are car oil/diesel burning activities including vehicles and generators [52,89,117].

Table 2.6: Measured acid gases concentrations during non-dusty and dusty days of the 2013 field campaign

Non-Dusty	HCl (μg/m^3)	HONO(μg/m^3)	HNO_3(μg/m^3)	H_2SO_4 (μg/m^3)	NO_2 (μg/m^3)	SO_2 (μg/m^3)
23-Jul-13	1.50	1.84	1.74	12.49	37.94	6.07
29-Jul-13	2.00	1.09	1.57	5.29	17.22	3.96
22-Aug-13	3.03	0.83	1.77	8.72	35.72	7.72
4-Sep-13	0.66	0.37	0.88	7.54	28.04	4.21
10-Sep-13	0.92	2.12	1.21	13.36	34.53	12.03
26-Nov-13	19.30	11.11	24.64	55.05		28.84
Dusty						
23-Oct-13	21.64	10.39	29.10	61.14	58.40	15.95
30-Oct-13	16.46	22.44	53.22	92.12	49.61	11.22
5-Nov-13	19.78	38.44	63.41	121.63	39.66	11.78
7-Nov-13	18.99	42.44	74.52	135.95	58.37	13.66
12-Nov-13	16.71	33.59	36.58	86.88	41.43	7.32
19-Nov-13	24.24	15.22	18.97	58.43	58.91	15.91

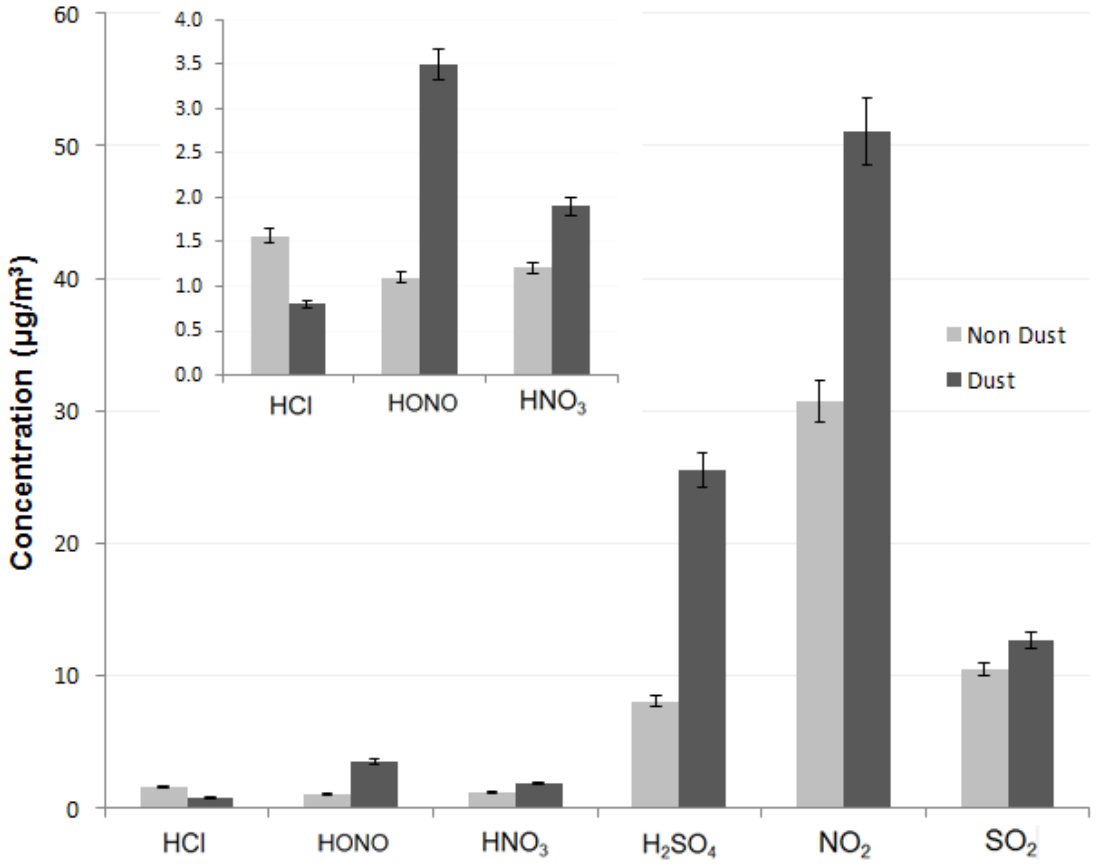

Figure 2.10: Bar graph showing the acidic gases concentration during non-dusty and dusty days. The insert is an enlargement of HCl, HONO and HNO_3

8. Nitrogen and Sulfur conversion factors

The extent at which these gases influence the content of particles in nitrates and sulfates is estimated by the conversion factors of nitrogen and sulfur species under different size distribution. The nitrogen conversion factor is defined by the ratio of nitrate that went into the particulate phase and is calculated following a modified version of the formula proposed by Khoder 2002 [118] as follows:

$$Fn = \frac{[NO_3^-]_p}{[NO_3^-]_p + [NO_3^-]_g + [NO_2]_g}$$

where F_n is the conversion ratio for nitrogen at various PM diameter sizes, $[NO_3^-]_p$ stands for the particulate nitrate concentration in $\mu g/m^3$, $[NO_3^-]_g$ represents the concentration of HNO_3 in the gas phase, and $[NO_2]_g$ represents the NO_2 concentration in the gas phase ($\mu g/m^3$).

During non-dusty days the average nitrogen conversion factor ratio was the smallest for the ultrafine diameter size (0.009) followed by the accumulation (0.018) then the coarse (0.06). This trend is explained by the abundance of nitrate particles in the coarse fraction (Fig 2.7). On dusty days as similar trend was noticed (Ratio CPM> Acc> UFP); however, the ratio for the ultrafine decreased to (0.007) while those for accumulation and coarse fractions increased to 0.029 and 0.085, respectively. The total PM_{10} nitrogen conversion factor also increased by 45% from 0.08 during non-dusty to 0.116 during dusty days. This is supported by the increase of nitrates during dust days (Fig. 2.7). This leads us to suggest an increase in the formation of secondary particles that could be due to an increase in NO_3^- precursors such as $HNO_{3(g)}$ and $NO_{2(g)}$ and/or the stagnant weather and the longer resistance time available for pollutants to interact[1].

The sulfur conversion factor calculation followed a proposed formula by Khoder 2002, [118] as follows:

$$F_{sd} = \frac{[SO_4^{2-}]_p}{[SO_4^{2-}]_p + [SO_2]_g}$$

where F_{sd} is the conversion ratio for sulfur at various PM sizes, $[SO_4^{2-}]_p$ is the particulate sulfate concentration ($\mu g/m^3$) at various sizes of PM, and $[SO_2]_g$ is the gaseous SO_2 concentration ($\mu g/m^3$).

Results (Table 2.7) show that during non-dusty, i.e. when the humidity is relatively high, the average conversion factor of sulfate is inversely proportional to diameter size as it is the largest for ultrafine mode (0.24) and the smallest for the coarse (0.08); reactions. During dusty days, on the other hand, this trend does not apply, decreases in the ultrafine and coarse fractions while increases in the accumulation mode to reach 0.35. These results are consistent with the particulate sulfate data and sulfate-ammonium correlation (Table 2.4 and reaction (16)), which show the sulfate increase in the accumulation mode during dust outbreaks.

Table 2.7: Nitrogen and Sulfur conversion factors for all size fractions and total PM during non-dusty and dusty episodes

	Nitrate Conversion Factor				Sulfate Conversion Factor			
Non-Dusty	**UF**	**Acc**	**CPM**	**Total PM**	**UF**	**Acc**	**CPM**	**Total PM**
23-Jul-13	0.006	0.023	0.056	0.081	0.378	0.310	0.103	0.540
29-Jul-13	0.019	0.034	0.070	0.115	0.417	0.102	0.196	0.518
22-Aug-13	0.006	0.015	0.051	0.070	0.383	0.154	0.085	0.473
4-Sep-13	0.009	0.012	0.067	0.085	0.196	0.505	0.044	0.567
10-Sep-13	0.007	0.006	0.066	0.077	0.080	0.134	0.054	0.229
26-Nov-13	0.010	0.016	0.029	0.053	0.007	0.035	0.017	0.057
AVERAGE	**0.009**	**0.018**	**0.062**	**0.080**	**0.243**	**0.207**	**0.083**	**0.397**
Dusty								
23-Oct-13	21.64	10.38	29.10	0.065	0.240	0.055	0.032	0.290
30-Oct-13	16.45	22.44	53.21	0.114	0.154	0.370	0.060	0.455
5-Nov-13	19.78	38.43	63.40	0.212	0.161	0.468	0.113	0.546
7-Nov-13	18.99	42.43	74.52	0.166	0.192	0.464	0.096	0.548
12-Nov-13	16.70	33.59	36.58	0.086	0.212	0.595	0.017	0.638
19-Nov-13	24.24	15.21	18.96	0.051	0.271	0.172	0.028	0.379
AVERAGE	**0.007**	**0.030**	**0.085**	**0.116**	**0.205**	**0.354**	**0.058**	**0.476**

D. Conclusion

Mass concentrations of coarse, accumulation and ultrafine PM size fractions increase during dusty days with the accumulation mode showing the highest percent increase of 72.60 %. The content of water soluble ions in PMs showed different trends of variations as a result of local emission sources, particle aging and chemical reactions between acidic gases and long range transported mineral dust particles. In particular, dusty days show a drastic decrease in the overall concentration of sea-salts ions in all size fractions coupled with an enhanced depletion of chloride. Non sea-salt crustal materials

such as magnesium and calcium exhibit increase in their concentration mainly in the coarse mode due to the influence of primary soil derived mineral dust particles and their interaction with acid gases like HNO_3 and H_2SO_4. The increase over non-dusty days of potassium was mostly concentrated in the accumulation mode due to the contribution of long range transport of biomass burning and agricultural activities to the levels of potassium in particles. In parallel, it was found, during dusty days, that the accumulation mode was also enriched with sulfate ions despite the fact that the ultrafine particles were most abundant with sulfates during non-dusty days. This phenomenon is in agreement with previous studies which show that sulfates during dusty days are mainly due to nucleation of $(NH_4)_2SO_4$ in the accumulation and ultrafine fractions. Since aerosol media in the different size fractions were found to be poor in ammonium, nitrates could not be abundantly associated with ammonium in the accumulation and ultrafine modes, rather its concentrations were most enhanced in the coarse fraction due the reaction of mineral dust particles with gaseous HNO_3 leading to Mg- and Ca- nitrates.

All acidic gases like HNO_3, H_2SO_4 and HONO except HCl experience an increase in acid concentrations during dusty days. The influence of these gases and their primary precursors NO_2 and SO_2 play a major role in the conversion of insoluble mineral dust particles into more water soluble nitrogen and sulfur components. It is shown that the coarse PM fraction is mostly affected in the nitrogen conversion whereas the PM accumulation fraction is the one enriched with soluble sulfate particles during dusty days.

This study of size segregated PM mass concentrations, during dusty days, has major implications on health as particle size and mass are directly linked to morbidity and

mortality. Furthermore, the assessment of PM chemical water soluble content of cations and anions at the different sizes help in understanding the nitrogen and sulfur deposition, soil acidification and biodiversity losses as a function of increased urbanization and aged particles.

CHAPTER III

CONTRIBUTION OF AIRBORNE DUST PARTICLES TO HONO SOURCES

A. Introduction

HONO is an important precursor for OH radicals in the atmosphere. Compared to ozone and formaldehyde, HONO photolysis is considered the major source of OH radicals in the early morning [1]. One of the main sources of HONO formation in the troposphere is attributed to the heterogeneous hydrolysis of NO_2 on wet surfaces (R1) [1] (and references therein) depicted by the mechanism shown in reactions (R2) to (R5).

$$NO_2 + H_2O \xrightarrow{surface} HONO_{(g)} + HNO_{3\,(particle)} \quad (R1)$$

$$2NO_2\,(g) \leftrightarrow N_2O_4\,(g) \quad (R2)$$

$$N_2O_4\,(g) \leftrightarrow N_2O_4\,(surface) \quad (R3)$$

$$N_2O_4\,(surface) \rightarrow ONONO_2\,(surface) \rightarrow NO^+NO_3^-\,(surface) \quad (R4)$$

$$NO^+NO_3^- \xrightarrow{H2O} HONO\,(g) + H^+ + NO_3^- \quad (R5)$$

This heterogeneous reaction has been studied on several underlying substrates such as soot, glass, mineral oxides and aerosol surfaces [82,119-123]. In urban regions, the reaction of NO_2 on surfaces is well known to be dependent on relative humidity [82] while the reactivity of the surface towards NO_2 is a function of other competing reactions such as the reaction of NO_2 in the presence of SO_2 on mineral surfaces [124]. As an example, TiO_2 nanoparticles which have been used in self-cleaning window glass, building materials, and on roads in Europe, Japan and the USA [125,126] are considered a source for HONO and H_2O_2 from NO_2 and H_2O. TiO_2 in dust was also shown to be a contributor to the formation of HONO [119,127]. Furthermore, modeling studies suggest that mineral aerosols surfaces account for 40% of nitrate formation and dust events create a favorable medium for the accumulation of nitrates [128-130]. The uptake of SO_2 on mineral oxide surfaces was shown to undergo a two-step mechanism including the reversible adsorption of SO_2 on the surface followed by the oxidation to sulfate [131]. In the case where SO_2 is co-adsorbed with NO_2 on the surface, it is shown that the oxidant is gaseous NO_2 which reacts with adsorbed SO_2 to produce sulfate in the particle phase. The oxidant role of NO_2 leads to nitrate or contributes to the formation of sulfate on the surface [119,132-134].

Given the reactivity of mineral oxide surfaces towards NO_2 and SO_2, some studies reported an increase of HONO levels during dust storms [133-136], however, the mechanism of HONO formation on airborne dust particles is still not understood. This study assesses the increase of HONO in the gas phase during Arabian dust, accompanied with aerosols at low relative humidity. Consequently, two mechanisms of actions for the formation of HONO during non-dusty and dusty episodes are proposed.

B. Methods

1. Sampling Location

Samples were collected on the roof-top of the Chemistry department at the American University of Beirut; North-West Beirut, Lebanon. The site is around 40 m above sea level. South of the site is the university's green belt of shrubbery and trees, and faces the Mediterranean Sea from the North. The location is considered to be an urban background site affected mainly by sea breeze; it is far from any industrial pollution sources and the closest roadway is located around 150 m north-east.

2. Collection techniques

Soluble gases and size resolved aerosols were sampled at ambient level during Arabian and African dusty and during non-dusty days. Dusty days were predicted using the NOAA-Hybrid Single Particle Lagrangian Integrated Trajectory (HYSPLIT) model of 48h isobaric backward trajectories [137]. HYSPLIT was run at three different altitudes between 1 and 5 km, the height of an average dust event. Arabian dust outbreaks have low initial heights (2 to 4 km) and show east and south-east trajectories, while African *dusty* episodes are carried by strong winds to higher elevations and have south-west backward trajectories [7,55]. Dust episodes were confirmed using BSC Dream Atmospheric Dust Forecast System. Wind speed and direction, local weather and visibility were used as other indications to the occurrence of dust-rich episodes.

The aerosol and gas samples are collected using a Rupprecht & Patashnick Partisol 2300. Sampling occurred between two different campaigns. Soluble acidic gases (HONO, HNO_3 and H_2SO_4) were sampled for 24hr using a diffusion denuder system. The system is based on two Honey Comb denuders (HC) coated with 1% $NaCO_3$ and 1% glycerol in 50:50 water: methanol solution and placed in series in Rupprecht & Patashnick (R&P) Chemcomb™ cartridges. Sampling and analysis of trace gases is fully described in Saliba and Chamseddine [22].

During the 2013 campaign (July-November 2013), PM sampling followed the procedure of Daher et al. [52]. Aerosols were sampled for 24hr using Sioutas Personal Cascade Impactor Samplers (Sioutas PCIS, SKC Inc., Eighty Four, PA, USA) preceded by denuder containing PM10 inlets and operating at 9 l/min. Dust particles were collected according to their size fractions; 10-2.5 μ m (coarse (CPM) particulate matter (PM)) and 2.5-0.25 μ m (accumulation (ACC) PM) were collected on 25mm Teflon filters and <0.25 μ m (quasi-ultrafine (UFP) PM) were collected on 37mm Teflon filters.

3. Ion Chromatography

Coated denuders are extracted by a 20mL of Deionized water. Each Teflon filter is extracted in 20 mL deionized water by sonication for 50 min at 80MHz. Both extracts are micro-filtered and analyzed by ion chromatography.

4. Gas Monitoring Station

The SO_2 and NO_2 gases levels in Beirut are monitored as discussed in Chapter II.

C. Results and Discussion

The average gas phase concentrations of HONO, HNO_3, and H_2SO_4 for the different sampling days are shown in Figure 3.1. It is noticed that a burst of HONO during dusty days is accompanied with an increase in HNO_3 and H_2SO_4 concentrations. Furthermore, this field campaign showed that the increase in HONO concentrations can be linked to an increase in gaseous NO_2 and SO_2 as shown in Figure 3.2. At the particle levels, both nitrate and sulfate showed, during dusty days, an increase in the concentrations of the different PM sizes; coarse, accumulation and ultrafine modes, over the non-dusty days (Figure 3.3). Considering the total cation and anion concentrations in the particulate phase, the acidity of the aerosols showed an increase in dusty over non-dusty days (Chapter II).

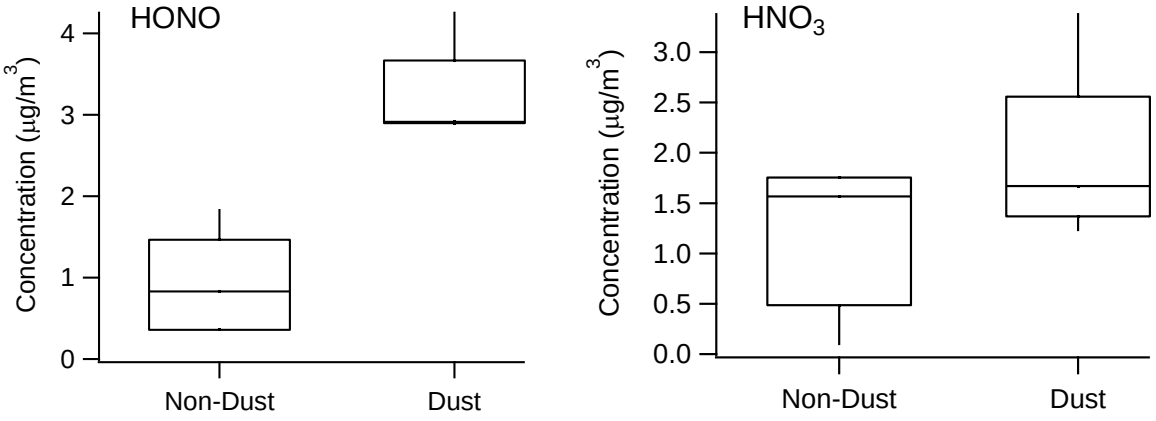

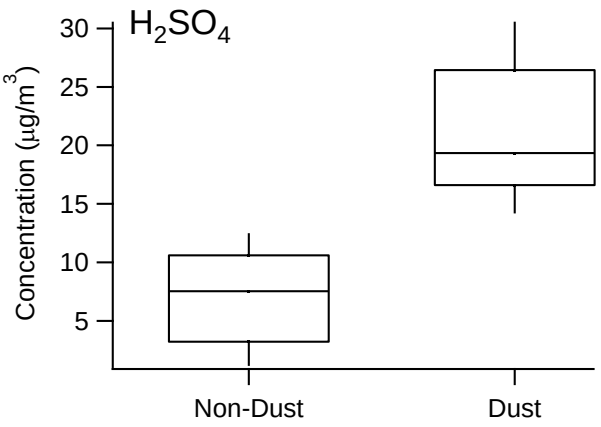

Figure 3.11 Box plot of the concentration of HONO, HNO_3 and H_2SO_4 during dusty and non-dusty days

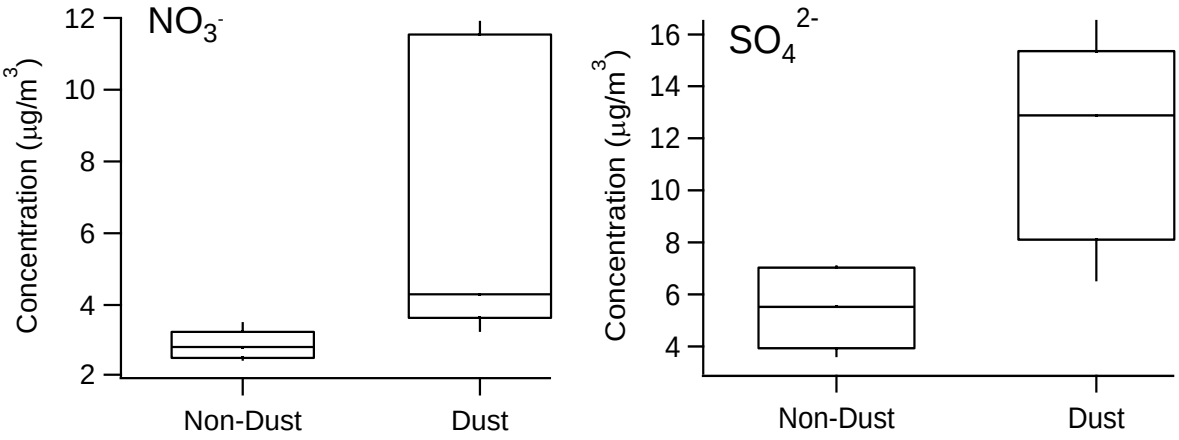

Figure 12 Box plot showing concentration of particulate phase nitrates and sulfates during dusty and non-dusty days

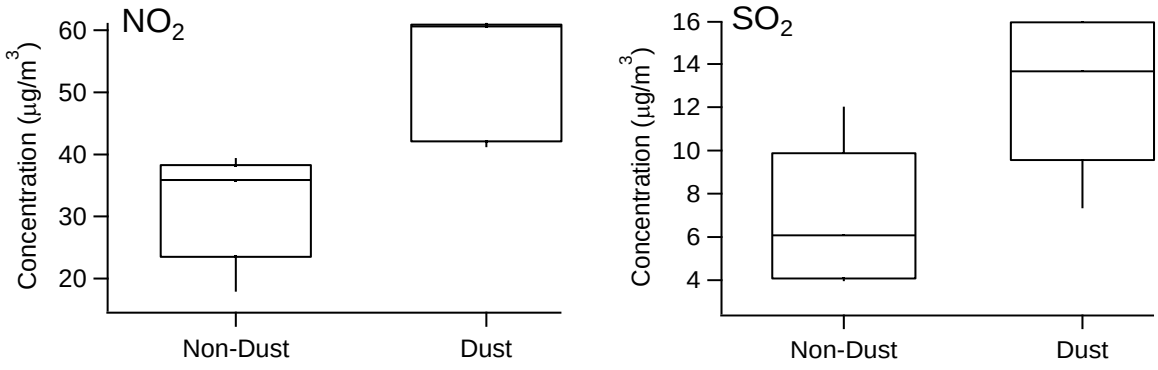

Figure 13.3 Box plot of concentrations of NO2 and SO2 during non-dusty and dusty days

During non-dusty days, it is noticed that high correlation between HONO and PM (ACC) ($R^2 = 0.80$), HONO and HNO_3 ($R^2 = 0.55$), and HONO and H_2SO_4 ($R^2 = 0.54$), indicate that most of these secondary acid gases and PMs originate from similar sources that are mostly local. Moreover, the high correlation between HONO and RH ($R^2 = 0.95$), and HONO and particulate NO_3^-(ACC) ($R^2 = 0.96$) suggests that the heterogeneous hydrolysis reaction (R1) is a contributing source to gaseous HONO and particulate nitrate formation.

During Arabian dust storms it is noticed that an increase in gaseous HONO, HNO_3 and H_2SO_4 concentrations is accompanied by the increase in their gas precursors; NO_2 and SO_2, respectively. This suggests that local emissions also contribute to the formation of acid gases in the atmosphere. However, the fact that the ratio of HONO/NO_2 and HONO/SO_2 doubled (0.03 vs 0.06 for HONO/NO_2 and 0.15 vs 0.30 for HONO/SO_2) despite the increase in NO_2 and SO_2 concentrations, suggests that there is an additional mechanism for the formation of HONO from NO_2. The heterogeneous hydrolysis of NO_2

cannot be considered a contributing source, in this case, because the air during these dust episodes is relatively dry (average RH ~ 30%) and the correlation between HONO and RH is low (R^2 = 0.15, with a negative slope). Furthermore, the low correlations between HONO and HNO_3 (R^2 = 0.01), and relatively lower correlation in comparison to non-dusty days between HONO and particulate NO_3^-(ACC) (R^2 = 0.57) confirm the low probability of this reaction during dusty days. Alternatively, enhanced are the correlations between HONO and the ratios of HONO/NO_2 (R^2 = 0.85 for dusty and R^2 = 0.50 for non-dusty days), HONO/SO_2 (R^2 = 0.99 for dusty and R^2 = 0.82 for non-dusty days), HONO/H_2SO_4 (R^2 = 0.93 for dusty and R^2 = 0.00 for non-dusty days), and HONO/HNO_3 (R^2 = 0.50 for dusty and R^2 = 0.10 for non-dusty days). These correlations suggest that, in addition to NO_2, SO_2 and its oxidized gaseous form H_2SO_4 play a role in catalyzing the formation of HONO in the atmosphere. Such synergy between SO_2 and NO_2 has been shown to exist in laboratory experiments. For instance, Ma et al. [138] showed that adsorption of NO_2 on alumnia was altered in the presence of SO_2. In similar studies, co-adsorption of SO_2 and NO_2 showed that the intermediate N_2O_4 leads to nitrates and sulfates in pathways different than the formation of $NO^+NO_3^-$ on the surface [124]. The extent of how much these laboratory experiments and consequently the depicted mechanism of HONO formation can be extrapolated to atmospheric reactions is yet to be proven with further studies.

D. Conclusion

The increase in HONO concentrations during dusty events has several implications on the OH concentration and oxidative budget in the atmosphere.

CHAPTER IV

ATMOSPHERIC MARKERS OF AFRICAN AND ARABIAN DUST IN AN URBAN EASTERN MEDITERRANEAN ENVIRONMENT, BEIRUT, LEBANON

A. Introduction

The increase in the total annual number of dusty days in the eastern Mediterranean is considered a result of local synoptic changes that are well documented and modeled in the region [11,13]. Based on a review of dust events in the past 49 years, an increasing trend of 0.27 days per year has been reported [14]. However, these dust events have various dust levels during different seasons and climax during winter and spring, rather than in summer [139]. Coupled to that, model predictions of the 21st Century reflect elevated summer temperatures and longer periods of heat waves [15]. The combination of higher frequency dust events with hot weather conditions is considered a favorable medium for homogeneous and heterogeneous photochemical processes which lead to higher concentrations of secondary organic aerosols and inorganic ions in particles. Organic matter transported from the desert, whether African or Arabian, has an economic impact as its depletion from the soil lowers agricultural productivity [140] . The implications of such events extend beyond the Mediterranean region and so understanding the changes of particle morphology and

chemical composition remain an important subject to investigate in different urban cities in the region.

Beirut can be considered an interesting city for the study of these phenomena as it connects the Mediterranean Sea from the west and an urban environment from the east. Beirut, among other Middle Eastern cities, experiences episodes originating from the Saharan and Arabian deserts [10]. For the Arabian episodes, these storms cross over various urban environments while Saharan dust crosses over the Mediterranean Sea. When dust particles mix with emissions from industrial and urban sites, it triggers morphological deformation of primary particles along with formation of new secondary ones.

This study explores the morphology and elemental composition of particles in Beirut during two *dust-rich* days originating from two distinct sources; Saharan and Arabian deserts. In order to identify specific markers for each trajectory, single particles collected during different dust episodes are compared. Results serve as basis for further research and modeling to assess the process of aerosol aging upon the mixing they encounter during their long-range transport.

B. Experimental and Analysis Methods

1. Sampling Location

Samples were collected on the roof of the Chemistry department at the American University of Beirut (AUB), situated approximately 20 m above the ground of the Chemistry building located at the North Western (NW) side of Beirut. More details about

the site can be found in Baalbaki et al. and Daher et al. [52,141]. The location of the site is shown in Figure 4.1.

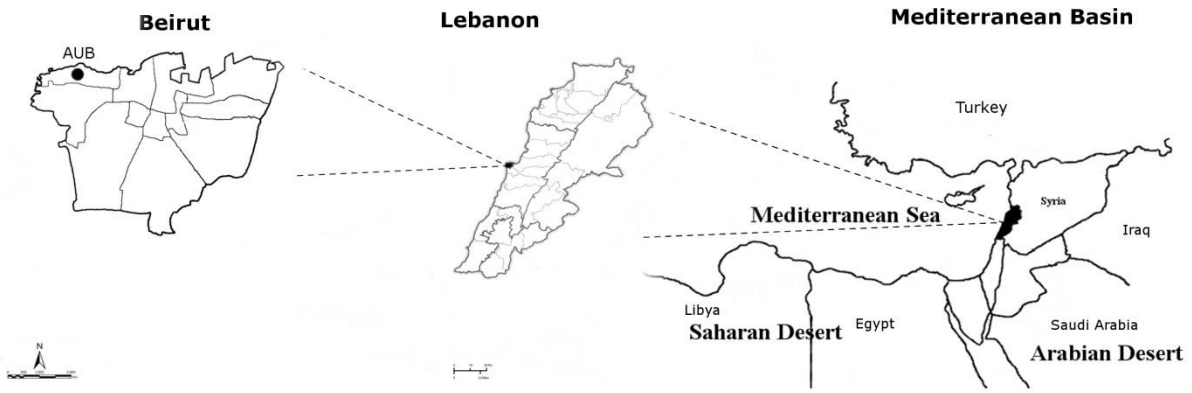

Figure 4.14 Sampling sites AUB

2. Sampling collection and Analysis

24h sampling periods were conducted at AUB during two different synoptic conditions. These were checked using HYbrid Single-Particle Lagrangian Integrated Trajectory (HYSPLIT) model of 48h backward trajectories between 900 and 2000 m: height of average dust event [53,54]. Saudi Arabian dust storms have low initial altitudes of 2–4 km, while Saharan dust can be elevated to much higher heights by strong According to Notaro et al. and references therein [142]. In our case, HYSPLIT was ran at the 3 different altitudes: 1.3716, 2.7432 and 11.5824 km. Outcomes showed that during African *dust-rich* episode on March 14, 2013 the air mass trajectories were found to be SW at all altitudes, proving the occurrence to be purely African. On the other hand, during Arabian *dust-rich* episode on November 22, 2012, air mass trajectories at lower heights (0.9144 – 3.0 km) were found to be E – SE and pertain to Arabian dust storm.

Samples were collected on aluminum stubs covered with 12 mm carbon adhesive tabs. These were mounted in a six-stage MPS-6 Microanalysis Particle Sampler cascade impactor of the following stage cut-off sizes: 10, 5, 2.5, 1.0, 0.5 and 0.1 µm. The instrument operated at flow rate of 2 $L.min^{-1}$. Samples were examined using Scanning Electron Microscopy (SEM) (Tescan Model 51-XMX0010) equipped with an Energy Dispersive X-ray system (EDX) for elemental identification. SEM operated at 20-30 KeV and 60 µA beam current, with spectral acquisition time of 60 sec. The diameter of the electron beam allowed the observation of the diameter of particles down to 0.1 µm. For each episode, coarse stages (1, 2 and 3) were examined. 50 particles from each were chosen, at random, to be analyzed for atomic weight percentage and are presented in Figure 4.2a.

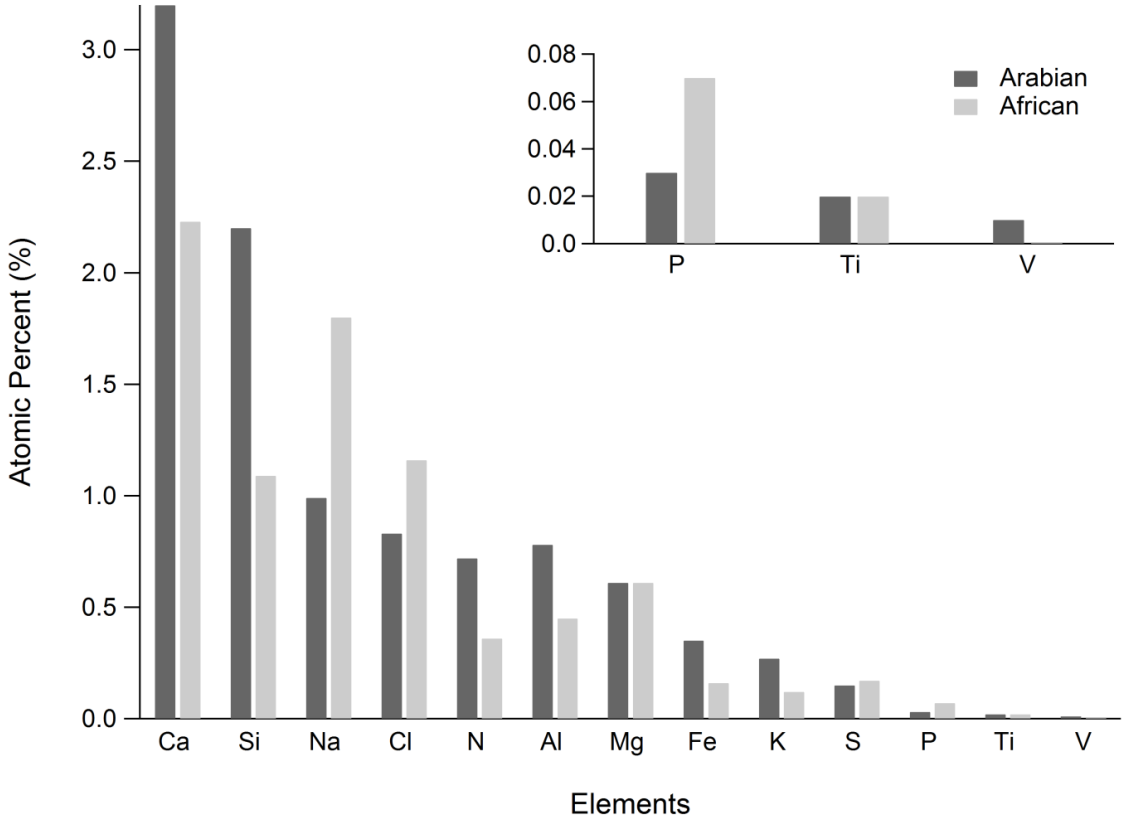

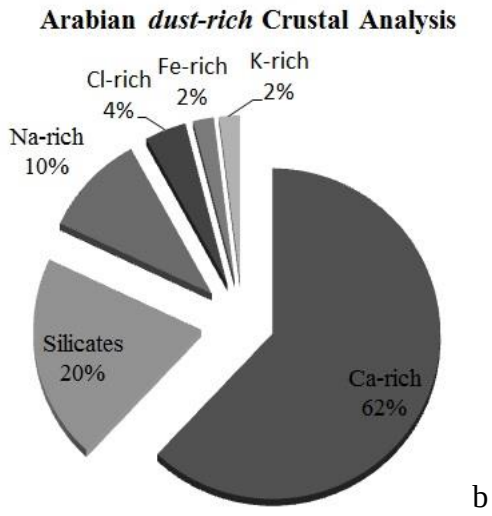

b

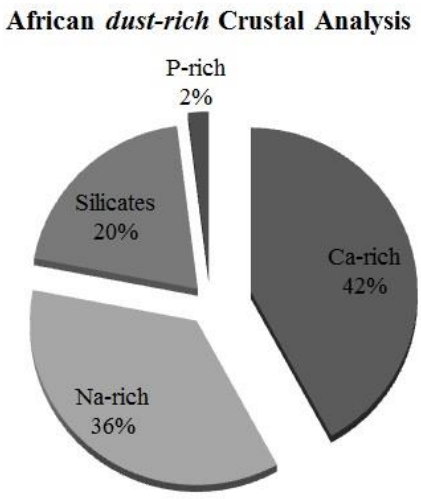

c

Figure 4.2 a) Percent occurrence of the elements identified in coarse single particles during dust-rich episodes. b) Crustal analysis of particles during Arabian dust –rich episode. c) Crustal analysis of particles during African dust-rich episode

C. Results and Discussion

Based on several studies conducted on local emissions [20,23,51,141,143-145], the main sources of pollution are traffic, construction sites, harbor activities and sea salts. The order of classification of these depends on the wind speed and direction at different sites. Minor emission has been related to industrial activities in the city of Beirut [146]. Several morphologies of carbonaceous species and aged sea salts were abundantly collected and characterized by SEM images and EDX analysis.

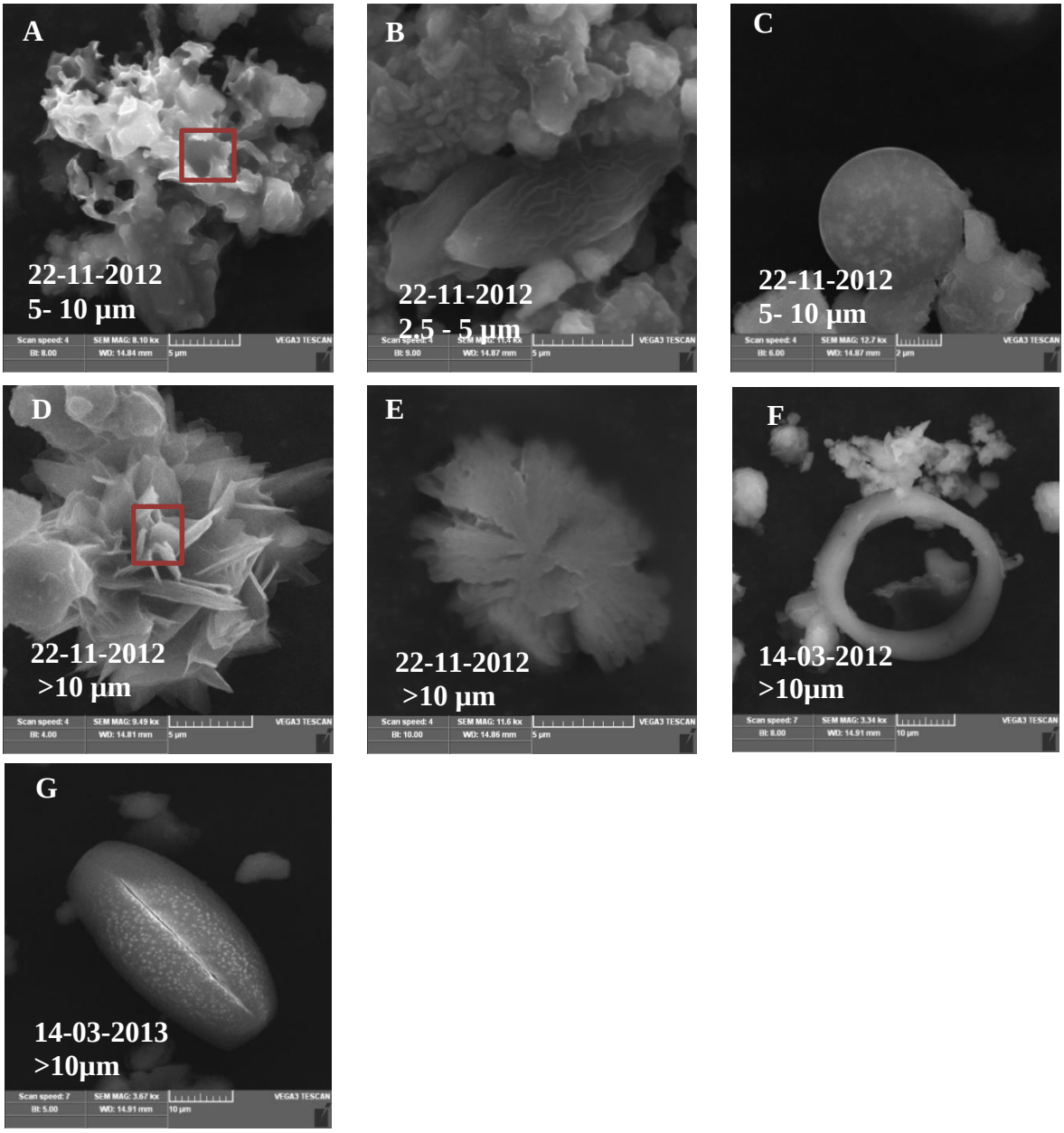

Figure 15 SEM images of particles collected during an Arabian *dust-rich* day (A to E), (A) $CaCO_3$ with vanadium traces, (B) Unidentified, (C) TiO_2 (D) Phosphorous oxide and (E) calcium and sodium nitrate and during an African *dust-rich* day (G to I). (F) Carbonaceous ring with sea salt mixture and (G) Carbonaceous dotted with P and S.

1. Unique morphologies of single particles collected during dust-rich Arabian day

Arabian dust is marked by high abundance of mineral crustal elements (Al, Si and Ca) and low amounts of sea-salts. Iron, which is also present in high amounts during these episodes, results in a reddish haze when in the form of oxides [8]. Furthermore, the high K content could be attributed to factors like biomass burning [76] and blowing dust [77]. Specifically, K identified as KNO_3 is a key ingredient in explosives and propellants [78]. These are collected along the way from the Arabian Desert to Lebanon crossing over Syria, where explosions are due to the current civil war. This suggestion is emphasized by traces of Titanium and Phosphorous oxides.

The most abundant particles of the Arabian dusty episode are irregular shaped particles of crustal elements. One distinguishes quartz, dolomite, and spherical aluminosilicates that are resistant to chemical modification [8]. Other spherical morphologies indicated the presence of fly ash particles, as well as TiO_2 and Fe_2O_3. These particles often derive from coal combustion and other metallurgical emissions [147]. Only unique morphologies of single particles apportioned to specific sources are illustrated in Figure 4.3 (A to E).

A particle mixture of Ca and V, shown in Figure 4.3A, contains traces of P and Si. It has an irregular unidentified morphology with soft edges and was not seen, up to our knowledge, in the region. Vanadium in aerosols was attributed to diesel fuel ash in other studies [148]. Since vanadium is only seen in Arabian *dust-rich* episodes, it serves as pointers towards Arabian Desert sources. Another particle composed of Si, O, and Ca mixed with sea salt particles has a rare oval shape as shown in Figure 4.3B. Uncommon particles such

as titanium and phosphorus oxides are shown in Figures 4.3C and 4.3D. TiO_2 shows a sphere-like structure (Figure 4.3C). Similar morphology was observed in northwest Madrid during an African dust episode [149]. Phosphorous oxide rods of sharp edges, form a flower-like cluster (Figure 4.3D), a morphology that has not been yet reported, up to our knowledge. Source of phosphorous in aerosols is normally attributed to biomass, fossil fuel and biofuel combustion and to other biogenic contributions, mainly volcanic and oceanic origins [150]. However, in this study, this specific shape of phosphorous oxide may be attributed to explosives in Syria. Finally a mixture of $NaNO_3$ and $Ca(NO_3)_2$, shown in Figure 4.3E, has a crystalline structure and is the result of the reaction of marine NaCl and $CaCO_3$ with atmospheric HNO_3 [151].

2. Unique morphologies of single particles collected during dust-rich African day

African desert episodes were differentiated by the abundance of sea salts and lower content of crustal elements and Fe. This indicates the marine layer contribution to aerosols from African Desert [13]. Furthermore, particles show low Ca content, despite the fact that Ca at the source (Saharan Desert) is higher than that of the Arabian [8]. In this study, it is confirmed that P, that is not in the phosphorous oxide form, marks the African dust [13]. Similar to Arabian Desert, traces of Mg, S and Ti were found, however in different morphologies.

During the African dusty day, morphologies different from those reported in similar episodes in the region are highlighted (Figure 4.3F and 4.3G). A ring-shaped carbon-rich particle mixed with sea salts (Figure 4.3F) is attributed to particles passing over the

Mediterranean. Although no similar morphology has been reported in ambient measurement, the particle resembles the experimental multiwall carbon rings resulting from coiling of carbon nanotubes by thermal decomposition of hydrocarbon gas [152]. Another remarkable carbonaceous particle of elongated morphology is dotted with P and S (Figure 4.3G). While sulfur is attributed to sea-salt spray [153], phosphorus originates from multiple anthropogenic (biomass burning and fuel emissions) and biogenic (mineral dust) sources. Phosphorous seems to adsorb on particle surfaces or associates with organic matter and is found to be a marker of Saharan dust outbreaks [13].

D. Conclusions

Subject to long range transport, particles originating from Arabian and African deserts undergo different chemical reactions which induce changes in their morphology and chemical composition. In addition to identifying interesting particle morphologies, this study focuses on markers that differentiate Arabian from African *dust-rich* episodes. In particular, the results show that Arabian *dust-rich* days are marked by traces of vanadium, crystal structures of aluminosilicate minerals, high abundance of Fe and the presence of phosphorous and titanium oxide crystals. These latter are ascribed to specific emission due to the Syrian civil war. On the other hand, Phosphorous mixed with carbonaceous species, deformed sea salt, and aged amorphous aluminosilicate particles all pointed to the contribution of Saharan dust in collected aerosols.

CHAPTER V

INFLUENCE OF DUST STORMS ON BACTERIAL COMPOSITION AND CONCENTRATION IN PM

A. Introduction

Bacteria are one type of bioaerosols that enter the atmosphere through anthropogenic and biogenic sources emissions including road-dust, vehicular emissions and agricultural activities [154-159]. The study of these microorganisms started in the late 1600s by the scientist Antony van Leeuwenhoek [160]. However, the real observation, assumptions and assessment started in the 1860s, when scientist Louis Pasteur related the presence of bacteria to health impacts [161].

Other than human health, airborne bacteria proved to have direct impacts on the economy including food and cosmetics contamination [162,163]. Air pollutants, especially atmospheric aerosols, are known for their association with short and long range transported airborne bacteria [164]. Once released into the air, the bacteria, due to their size, can remain suspended until further wet removal or direct deposition [165], the fact that raised speculations regarding the interaction of these bacteria between the atmosphere and the earth's surface. The importance lies within the impact of the suspended bacteria on the chemistry and global distribution of clouds and precipitation [165-188].

Furthermore, bioaerosols are carried upwards by current winds and can be transported to distances from some to several kilometers [165,189-191]. The variation in the bacterial communities is dependent on the physical and chemical characteristics of the associated aerosol. The survival and distribution of these is, also, highly dependent on the meteorological conditions [154,162]. For all factors mentioned, the study of the effect of different environmental and synoptic conditions on bacterial count and species is important. Many studies have related bacterial properties to long range transport or dust events [154,164,191-193]. However, very few studies in the Mediterranean region, up to our knowledge, have reported comparative data related to bacterial concentrations and diversity during Arabian and African dust-outbreaks [194,195].

Desert storms, which release around 2 billion metric tons of dust into the atmosphere, annually, have been related to increased probability of biological material, containing spores, bacteria, pollen and others [154,196]. Since Beirut lies at an intersection of several cross roads susceptible to different dust-outbreaks from the Arabian and African Deserts, the study of biological aerosols during each is possible. Also, previous studies done in our lab presented SEM images of spores collected during non-dusty episode which triggered the initiation of the current study (Fig 5.1)[7]. Therefore, the present study aims to measure bacterial content in PM_{10} associated with Arabian and African dust storms and compare it to bacterial concentrations collected during non-dusty days.

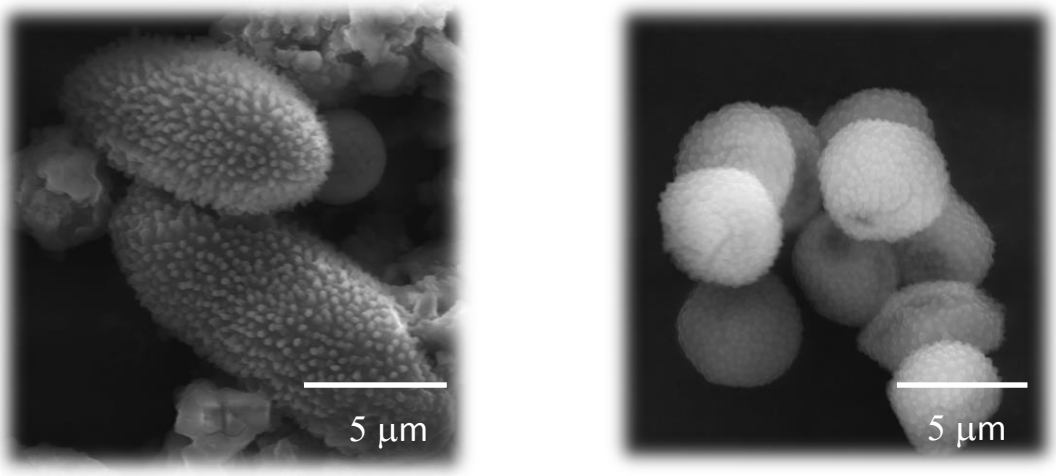

Figure 5.16 SEM images of spores collected during non-dusty episodes

B. Materials and Methods

1. Description of the sampling site

Sampling was conducted at the roof top of the Chemistry Department at the American University of Beirut; North-west Beirut, Lebanon. Mostly, the site is surrounded by the green university belt of trees and shrubbery, with mostly pedestrian rails. This location is an urban background site, affected mainly by sea-breeze. The fact that the location is far from direct industrial and vehicular emissions makes the site ideal for the assessment of the effect of the two different dust storms on the aerobic bacterial content. Also, the location of the site is 40 m above sea level and is far from any construction site, allowing the assessment of yeast and mold associated with dust. Further description of the site is detailed by Baalbaki et al. 2013 and Daher et al. 2013 [18,52] and its location is shown in Fig. 5.1.

2. Characteristics of backward air masses

HYbrid Single-Particle Lagrangian Integrated Trajectory (HYSPLIT): 48h air mass backward trajectories for all sampling days were checked using NOAA-HYSPLIT model [53,54] for the predicition of dusty and non-dusty days. One model run per sampling day was considered for all sites, as sites are within few kilometers away from each other. HYSPLIT was run at three different altitudes between 1 and 10 km, the height of an average dust event. Samples were collected during Arabian dust outbreaks, which have low initial heights (2 to 4 km) and show east and south-east trajectories [7,55]. One the other hand, Saharan dust can be lifted to heights of several kilometers above the ground due to strong winds and show south-west trajectories [197-200]. Dusty days were confirmed using BSC Dream Atmospheric Dust Forecast System. Wind speed and direction, local weather and visibility were used as other indications to the occurrence of dusty days.

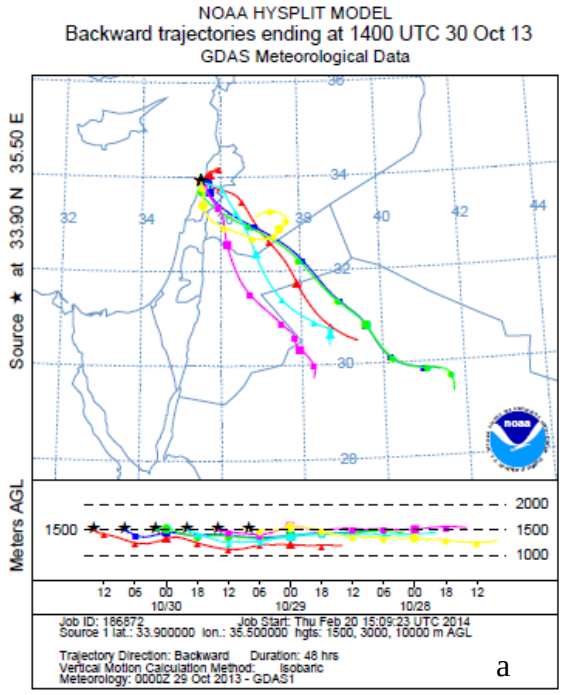
NOAA HYSPLIT MODEL
Backward trajectories ending at 1400 UTC 30 Oct 13
GDAS Meteorological Data
Source ★ at 33.90 N 35.50 E
Meters AGL
Job ID: 186872 Job Start: Thu Feb 20 15:09:23 UTC 2014
Source 1 lat.: 33.900000 lon.: 35.500000 hgts: 1500, 3000, 10000 m AGL
Trajectory Direction: Backward Duration: 48 hrs
Vertical Motion Calculation Method: Isobaric
Meteorology: 0000Z 29 Oct 2013 - GDAS1
a

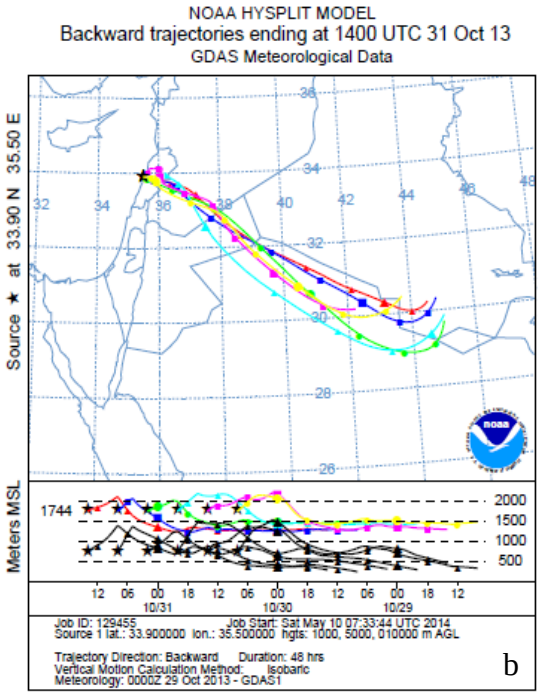
NOAA HYSPLIT MODEL
Backward trajectories ending at 1400 UTC 31 Oct 13
GDAS Meteorological Data
Source ★ at 33.90 N 35.50 E
Meters MSL
Job ID: 129455 Job Start: Sat May 10 07:33:44 UTC 2014
Source 1 lat.: 33.900000 lon.: 35.500000 hgts: 1000, 5000, 010000 m AGL
Trajectory Direction: Backward Duration: 48 hrs
Vertical Motion Calculation Method: Isobaric
Meteorology: 0000Z 29 Oct 2013 - GDAS1
b

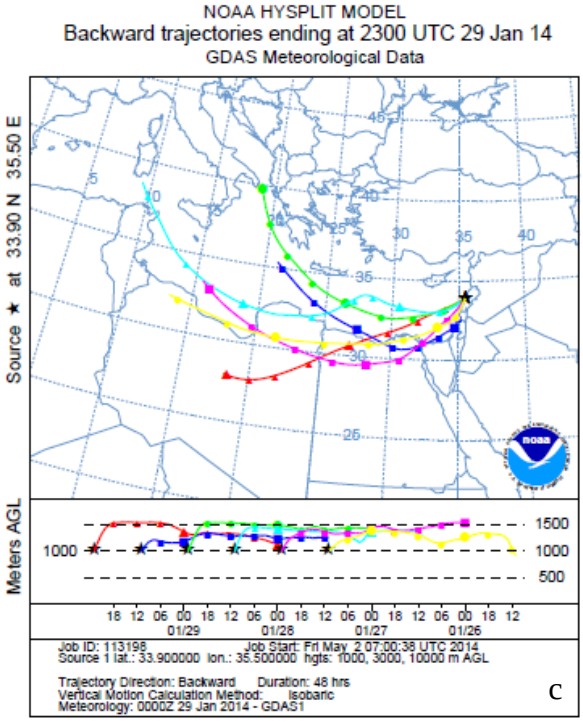
NOAA HYSPLIT MODEL
Backward trajectories ending at 2300 UTC 29 Jan 14
GDAS Meteorological Data
Source ★ at 33.90 N 35.50 E
Meters AGL
Job ID: 113198 Job Start: Fri May 2 07:00:38 UTC 2014
Source 1 lat.: 33.900000 lon.: 35.500000 hgts: 1000, 3000, 10000 m AGL
Trajectory Direction: Backward Duration: 48 hrs
Vertical Motion Calculation Method: Isobaric
Meteorology: 0000Z 29 Jan 2014 - GDAS1
c

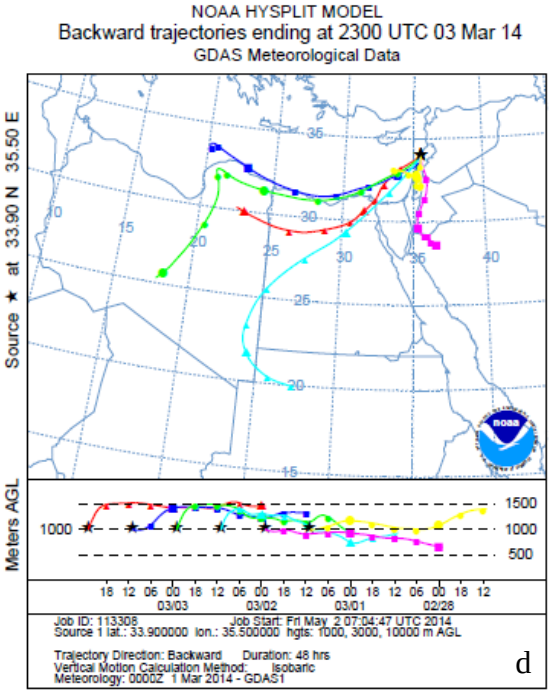
NOAA HYSPLIT MODEL
Backward trajectories ending at 2300 UTC 03 Mar 14
GDAS Meteorological Data
Source ★ at 33.90 N 35.50 E
Meters AGL
Job ID: 113308 Job Start: Fri May 2 07:04:47 UTC 2014
Source 1 lat.: 33.900000 lon.: 35.500000 hgts: 1000, 3000, 10000 m AGL
Trajectory Direction: Backward Duration: 48 hrs
Vertical Motion Calculation Method: Isobaric
Meteorology: 0000Z 1 Mar 2014 - GDAS1
d

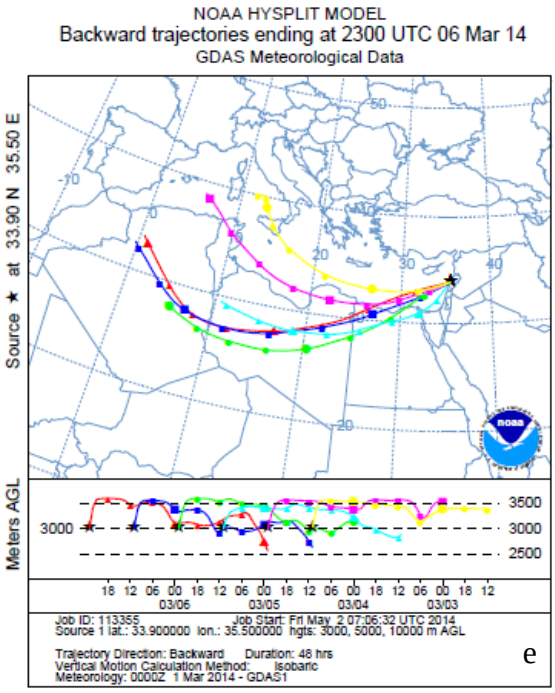
NOAA HYSPLIT MODEL
Backward trajectories ending at 2300 UTC 06 Mar 14
GDAS Meteorological Data
Source ★ at 33.90 N 35.50 E
Meters AGL
3500
3000
2500
03/06
03/05
03/04
03/03
Job ID: 113355 Job Start: Fri May 2 07:06:32 UTC 2014
Source 1 lat.: 33.900000 lon.: 35.500000 hgts: 3000, 5000, 10000 m AGL
Trajectory Direction: Backward Duration: 48 hrs
Vertical Motion Calculation Method: Isobaric
Meteorology: 0000Z 1 Mar 2014 - GDAS1
e

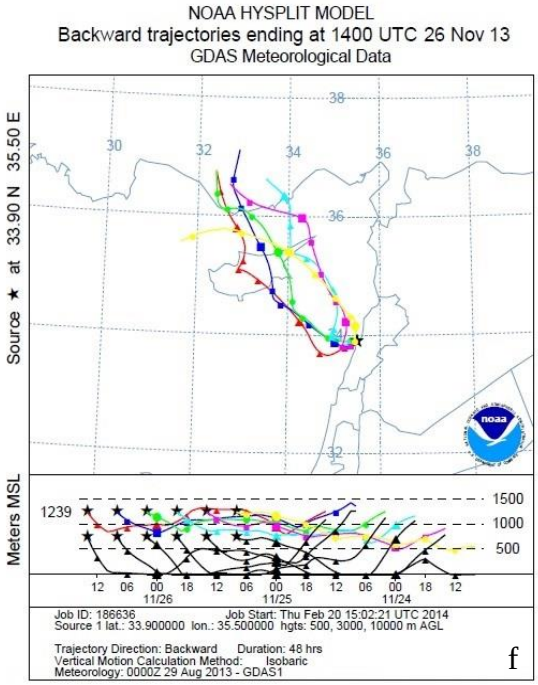
NOAA HYSPLIT MODEL
Backward trajectories ending at 1400 UTC 26 Nov 13
GDAS Meteorological Data
Source ★ at 33.90 N 35.50 E
Meters MSL
1239
1500
1000
500
11/26
11/25
11/24
Job ID: 186636 Job Start: Thu Feb 20 15:02:21 UTC 2014
Source 1 lat.: 33.900000 lon.: 35.500000 hgts: 500, 3000, 10000 m AGL
Trajectory Direction: Backward Duration: 48 hrs
Vertical Motion Calculation Method: Isobaric
Meteorology: 0000Z 29 Aug 2013 - GDAS1
f

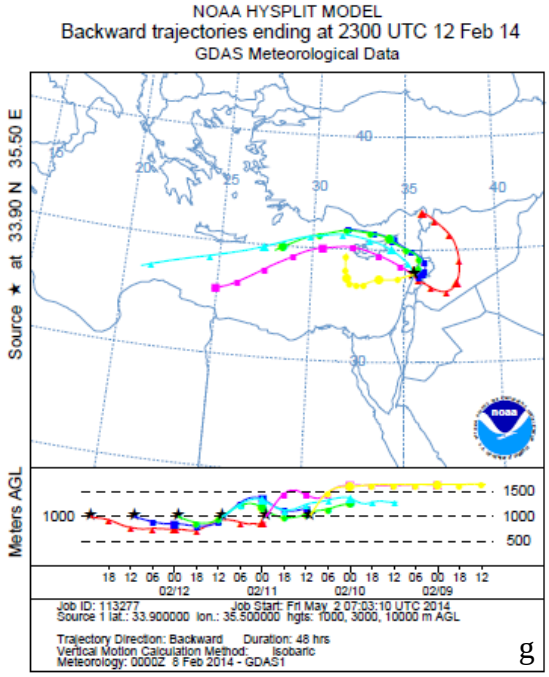
NOAA HYSPLIT MODEL
Backward trajectories ending at 2300 UTC 12 Feb 14
GDAS Meteorological Data
Source ★ at 33.90 N 35.50 E
Meters AGL
1000
1500
1000
500
02/12
02/11
02/10
02/09
Job ID: 113277 Job Start: Fri May 2 07:03:10 UTC 2014
Source 1 lat.: 33.900000 lon.: 35.500000 hgts: 1000, 3000, 10000 m AGL
Trajectory Direction: Backward Duration: 48 hrs
Vertical Motion Calculation Method: Isobaric
Meteorology: 0000Z 5 Feb 2014 - GDAS1
g

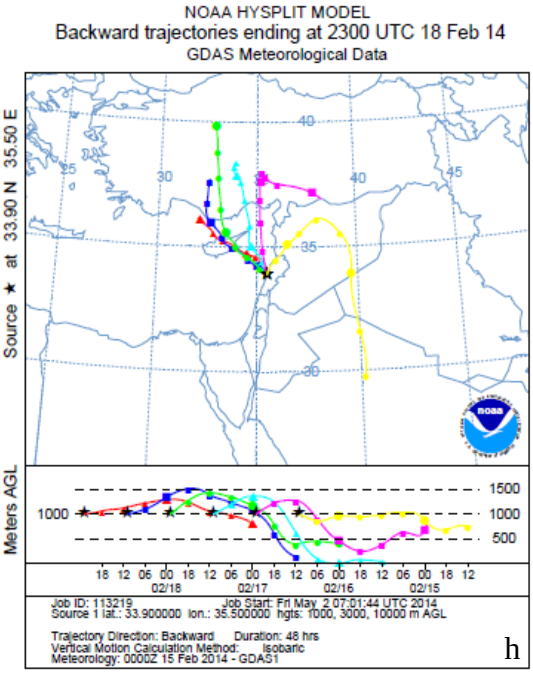
NOAA HYSPLIT MODEL
Backward trajectories ending at 2300 UTC 18 Feb 14
GDAS Meteorological Data
Source ★ at 33.90 N 35.50 E
Meters AGL
1000
1500
1000
500
02/18
02/17
02/16
02/15
Job ID: 113219 Job Start: Fri May 2 07:01:44 UTC 2014
Source 1 lat.: 33.900000 lon.: 35.500000 hgts: 1000, 3000, 10000 m AGL
Trajectory Direction: Backward Duration: 48 hrs
Vertical Motion Calculation Method: Isobaric
Meteorology: 0000Z 15 Feb 2014 - GDAS1
h

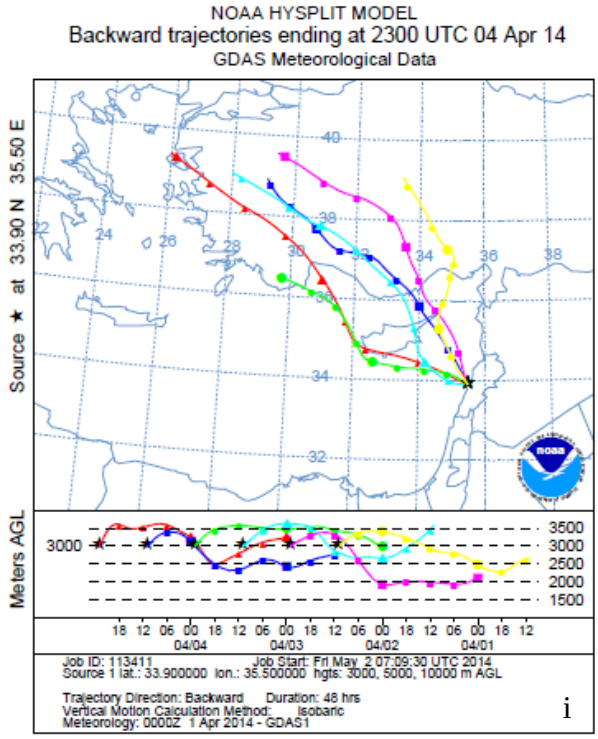

Figure 5.2 NOAA-HYSPLIT air mass trajectories showing: a-b) east and south east trajectories typical of Arabian dusty day c-e) south-east trajectories indicative of African dust storm and f-i) north and north-west trajectories demonstrating non-dusty wind

3. Aerosol Sampling

Samples for the airborne aerobic cultural bacterial concentrations where collected for 24 hours during different dust episodes between October 2013 and April 2014. A high-volume air sampler (DIGITEL DH77) operating at a flow rate of 250 l/min was used to collect particulate matter, diameter 10 µm and below, on baked 150 mm quartz filters.

To remove any bacterial contamination, the filters and the aluminum foil used for storage, were baked at 450℃ for at least 12hrs and frozen at -20℃ prior to sampling. After sampling (Fig. 5.3a), filters were placed in baked aluminum foil and stored in a freezer at -

20℃ until further extraction. For extraction, the sample filters were transported and cut, into 4 quarters where 2 quarters are used for bacterial assessments as duplicates (Fig. 5.2c).

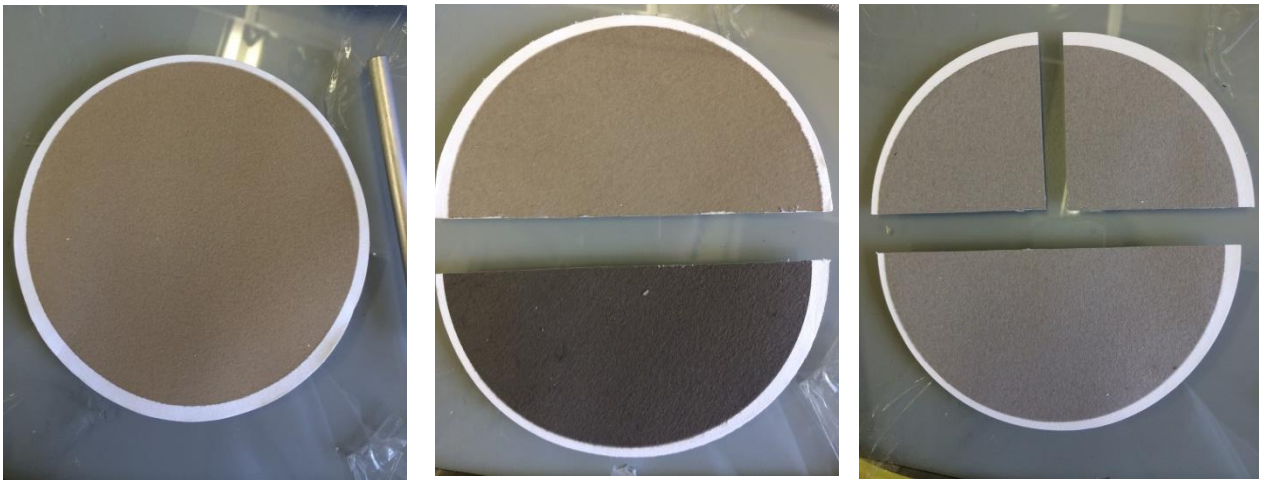

Figure 5.2 a)African dust collected on 150 mm quartz filter.b) African dust filter (top) and Arabian dust filter (bottom) each cut in half. c) PM_{10} collected on filter during non-dusty day showing cuts into quarters.

4. Extraction procedure

a. Materials

Peptone water (Bio-rad 356-4684) was prepared by dissolving 20g of the powder in 1L of distilled water, heated to homogenize and autoclaved at 121℃ to sterile as recommended by the accompanying manual

b. Culture agar plates

Total aerobic bacteria were enumerated on plate-count agar (PCA) (Bio-rad 356-4475) while yeasts and molds were identified on yeast glucose chloramphenicol agar (256-4104). *Bacillus Cereus* were cultured on Mossel (MYP: Mannitol egg yolk

Polymixin/Agar) (BC) (Bio-rad 356-9604). Total coliforms and Escherichia coli were differentiated and enumerated on RAPID'E.coli 2 agar (REC) (356-4024) by the pour-plate technique [201].

5. Methods

Prior to extraction, each quarter filter was transported into a sterile stomacher bag and weighed. Based on the weight, a certain volume of the peptone water was added to completely soak the filter. The bag is then placed in the stomacher for 2 min.

Around 10 ml of the supernatant sample was pipetted and transferred to a 15ml conical flask (Fig.5.3a). 0.1 ml was then pipetted to each agar plate (PCA, BC and YGC) (Fig. 5.3b) and spread using a sterile glass spreader (Fig. 5.3c) via the spread-plate technique [202]. Another, 1ml was pipetted to an empty pour plate for E.coli and coliforms analysis (Fig. 5.3d). REC agar was added to these plates and left to cool to room temperature and harden via the pour-plate technique [201]. A duplicate plate was performed for each.

Prior to colony count, all plates (PCA, BC and REC), except the YGC, were placed in a 37℃ incubator for 24hours. The YGC plates are kept at room temperature in a dry environment for 3 to 5 days.

All grown colonies were visible to the naked eye and were less than 250 in number, hence easily counted. The bacterial concentration was calculated as the number of colony forming units per 1 g of dust (CFU/g) as follows[203]:

$$\text{Bacterial concentration (CFU/g)} =$$

$$\text{average number of colonies} \times \frac{1}{\text{Dilution factor x amount plated}}$$

Where the average number of colonies between the two duplicate plates is considered, the dilution factor (g/ml) is the mass of dust divided by the soaking volume of peptone water and the amount spread on the plate is 0.1 ml for all plates (PCA, BA, BC and YGC), except for REC where 1ml is added.

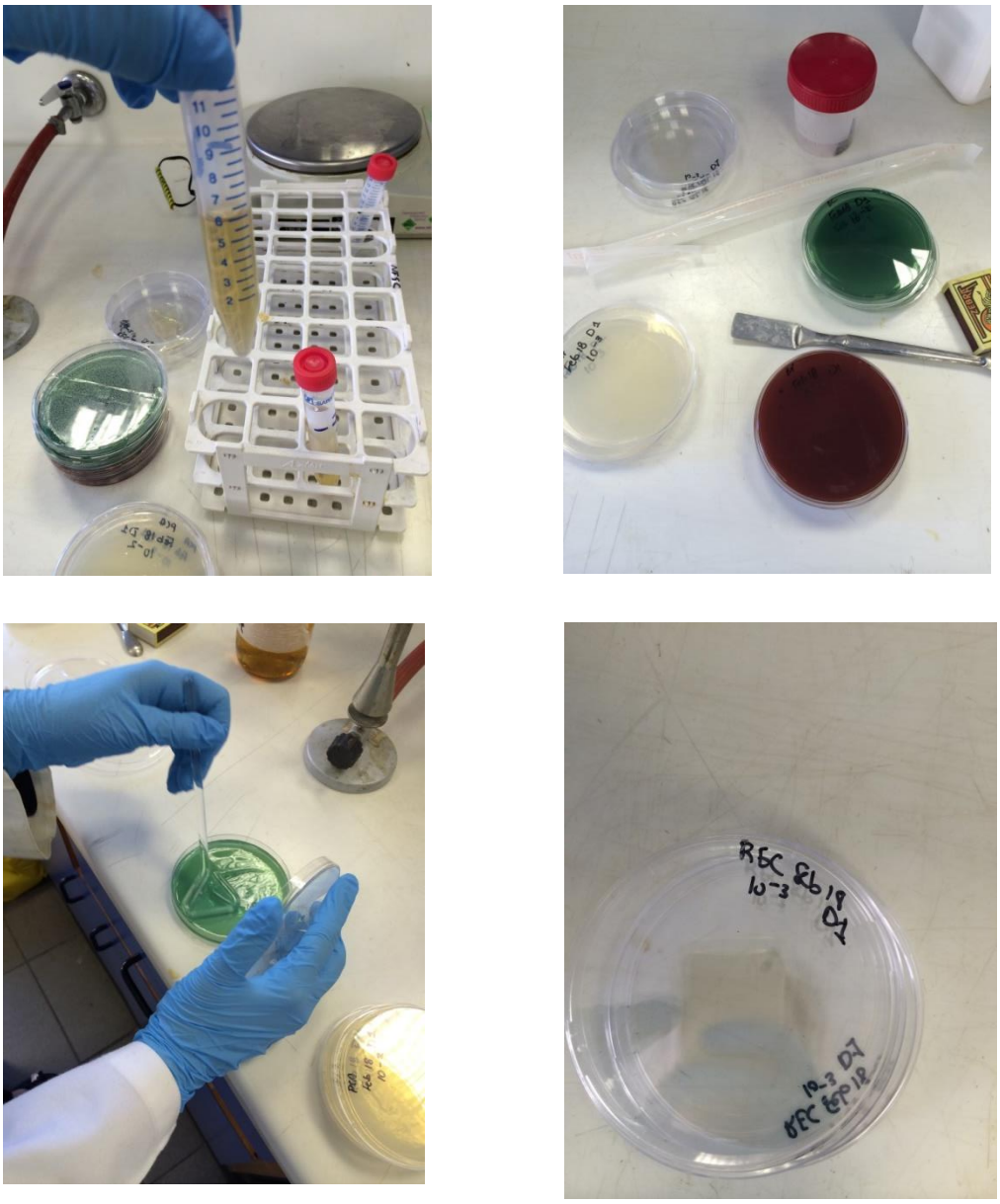

Figure 17 a) Filter extract b) filter extract on agar c) spreading of filter extract d) REC pour plates

C. Results and discussion

Bacteria associated with dust

Several studies criticized cultural techniques of airborne bacterial concentration, where the bacteria are left to enumerate in situ in the outdoor harsh conditions [164,204-206]. Therefore, in the current study, the bacteria collected during different synoptic conditions is left to grow and proliferate in optimum conditions which rules out the possibility of underestimating the bacterial concentration.

The biological loading of airborne bacteria and yeasts and molds in 9 PM_{10} filters were studied. In Table 1 are summarized the averages of the total aerobic bacteria (TAB (CFU/m^3)), Bacillus Cereus (BC (CFU/m^3)), Yeasts and molds (YGC (CFU/m^3)), along with the averages of particulate matter with diameter <10 (PM_{10} (μg/m^3)). Results show that regardless of the weather conditions, non-dusty, Arabian, or African dusty episodes, the yeast and mold concentrations were the highest between all tested bioaerosols. Among the three different environments the measured concentration was highest during Arabian dusty days (1099 CFU/m^3) which is 44.5% and 34.5% higher than the African and non-dusty, respectively. Our results were consistent with other reported results in the region [207], which show an increase in total fungal concentrations during dust events in comparison to non-dusty. The mean yeasts and molds concentration found in our study is 58% higher from what is reported in the city of Athens. In comparison to other cities around the world, high concentrations of airborne fungi are characteristic of this geographic region. It is also higher in comparison to bacteria [208-210]. Unlike Griskhan et al. 2012 and Schlesinger et al. 2006 who presented airborne fungal data from Haifa, Israel in 2006, our data did not show

a significant difference in the fungal count between non-dusty and dusty days, although we measured similar concentrations at times [194,195].

Total aerobic bacteria enumerated on PCA, a favorite medium for bacterial, are highest during African dusty days (472.8) followed by the non-dusty (167.3) and Arabian dusty days (165.4). These results can be attributed to an increase in relative humidity [211]. Also, the increase of bacterial count during African dust might be attributed to the passage of air mass over the Mediterranean Sea carrying along marine aerosol-associated bacteria [165]. Bacteria are known to be negatively affected by the long range anthropogenic pollution [164,212,213], which might explain the decrease of bacterial concentration during Arabian dust storms, which pass over arid urban environments. Furthermore, *Bacillus Cereus* which are one dominant specie of airborne bacteria [154], shows an average of 763 CFU/m^3 during Arabian dusty days, a much higher concentration in comparison to 161 and 145 for non-dusty and African dusty days, respectively. Although Bacilli do not have adverse human health effects [214], it has been shown that these accompany soil composting processes[215] and other vegetation activities[216].

As shown in Fig 5.5, daily variations in the amount of airborne bacteria and fungi do not show a clear trend that could be attributed to one of three different environmental conditions. This is a normal behavior of large temporal variation in the airborne bacterial and fungal concentrations that has been reported in many different studies. Unlike other studies, this variation was not found to be related to PM mass concentration as reported in other studies [208,217,218].

Escherichia coli and coliforms were absent in all the tested samples, although some literature reports the association of these strains to particulate matter [219,220].

Table 5.1: Total aerobic bacteria, Bacillus Cereus, Yeasts and molds, and particulate matter with diameter <10 (PM_{10})

	Non Dust	Arabian	African
TAB (CFU/m^3)	167.3 ± 165.4	165.4 ± 143.7	472.8 ± 550.0
BC (CFU/m^3)	120.8 ± 241.3	1.0 ± 1.4	0.7 ± 0.5
YGC (CFU/m^3)	817.5 ± 964	1099.3 ± 1022.4	760.8 ± 447.2
PM_{10} ($\mu g/m^3$)	98.2 ± 49.2	164.7 ± 32.0	189.6 ± 92.9

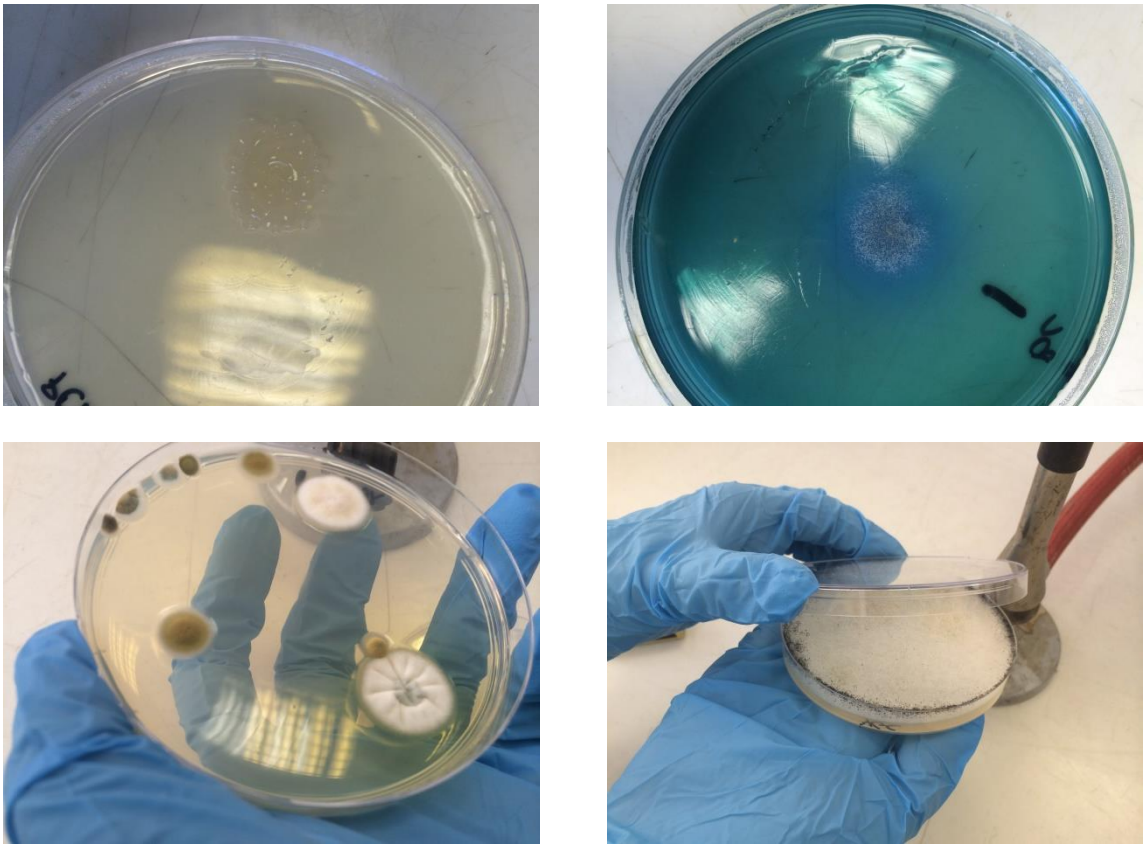

Figure 18: Growth of Bacteria (a) TAB (b) BC (c-d) Yeasts and molds

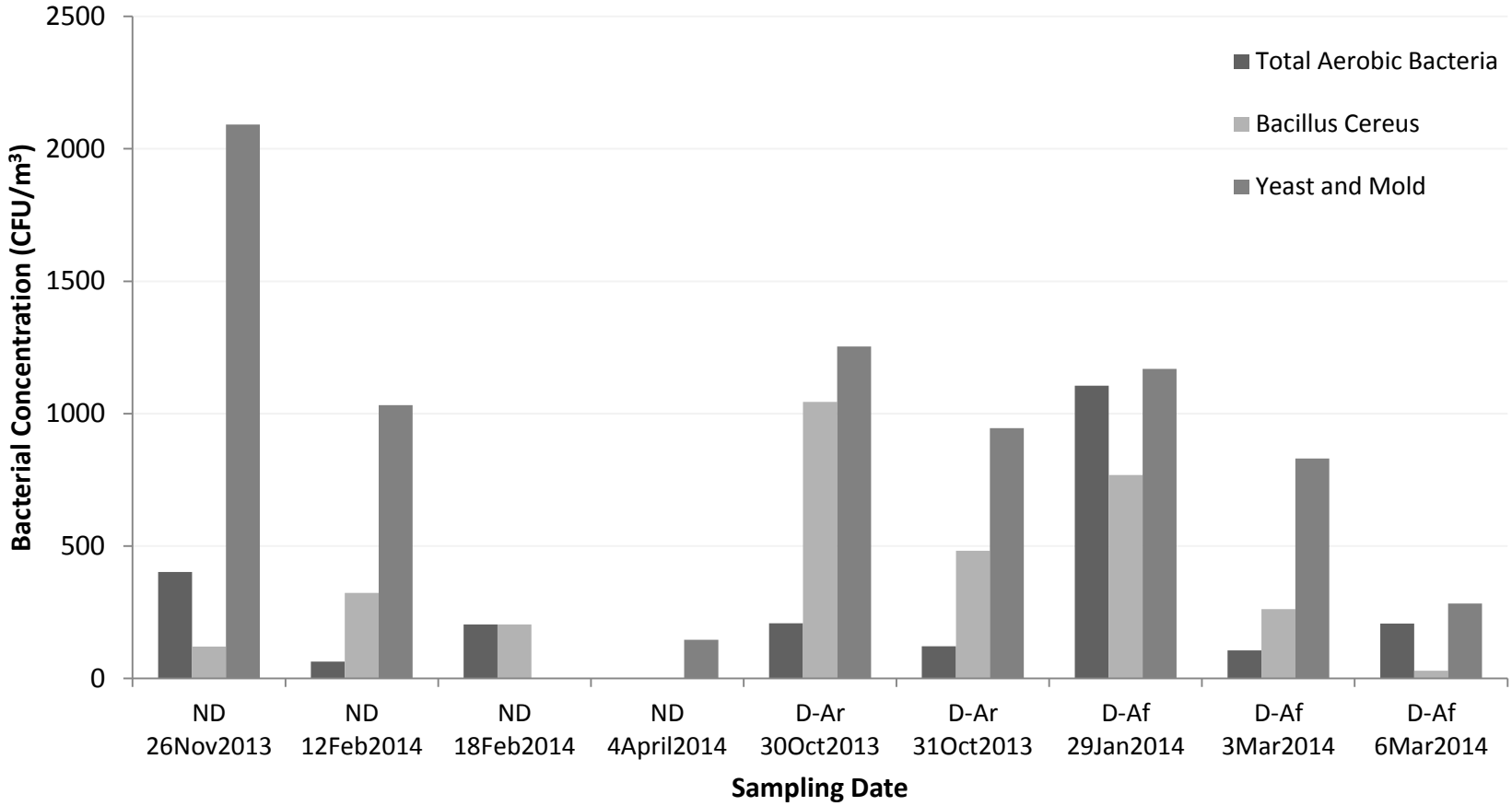

Figure 19 Daily variation of bacterial concentration (Total aerobic, bacillus cereus and yeasts and molds) during non-dusty (ND), Arabian dusty days (D-Ar) and African dusty days (D-Af).

D. Conclusion

This preliminary study presents the total aerobic bacterial concentration in CFU/m^3 as well as yeast and mold concentration in PM_{10} collected in Beirut during non-dusty and during Arabian and African dusty days. Bacteria did not show follow a trend between dusty and non-dusty days in daily variations. Yeasts and molds yield high concentration during non-dusty stagnant environments which is a characteristic of our region. Further studies are needed to assess the bacterial count and trends.

CHAPTER VI

CONCLUSION

For the eastern Mediterranean dust episodes probability increases from fall to winter. A peak is usually observed in April, after which it decreases sharply toward summer [221].In spring (March–May), dust episodes are mainly due to African South-East Westely wind, and in the Fall (September–November) to Easterly wind originating from the Arabian Desert [222]. Moreover, dust in the two events, is reported to have distinct difference in the particle size distributions[222] and that most particles originating from soils and sediments are either polluted at the origin or along their transport with high proportions of urban pollution[223]. Origin and long range contamination influence the particle aging and consequently their sizes as well as the gas-particle partitioning of the different chemical components. In this study we only considered the PM size segregation and water soluble ions due to their importance on the cloud condensation and radiative properties and on their effect on rendering mineral dust particles more soluble and hence more available to the ecosystem.

In non-dusty days, ammonia readily reacts with sulfuric acid in the ultrafine mode to form non-volatile and neutralized ammonium sulfate which could be present in the form of sulfate and bisulfate. In dusty days, it was found that ammonium sulfate was enriched in the accumulation mode rendering these particles more prone to condensation and formation of bigger particles affecting absorption of aerosols to incoming solar radiation on the one hand, and on the other hand, more available for particle wet and dry deposition on the earth and ocean

surfaces and leach out of iron present along sulfates in the particles. In fact, the difference in iron solubility in particles was shown to depend on bulk sulfate content and not on iron content in fine particle samples (PM2.5) in Atlanta[224].

Moreover, the increase in nitrate concentrations, during dusty days, in the coarse fractions has been attributed to the homogeneous reaction of HNO_3 with basic components of mineral dust such as $CaCO_3$ or to heterogeneous reactions of primary $NO_2(g)$ with water surfaces at high relative humidity to produce HONO(g) and HNO_3(particles). The formation of $Ca(NO_3)_2$ also impacts the solubility of particles and $Ca(NO_3)_2$, thus decreasing the pH of the aerosol and increasing its solubility [4,225-227]. $Ca(NO_3)_2$ deliquesces at a relative humidity (RH) lower than the typical environmental RH values (9 - 11%), which increases solubility of the aerosol [228]. Upon deposition of mineral dust aerosols onto vegetation or marine surfaces, soluble fractions of Fe, N and P can be utilized as nutrients[228-230]. Further, in the Mediterranean region, change in dust-bound soluble nitrogen deposition has been recognized to be a main driver of changes in the composition of prevalent vegetation species. In particular, elevated nitrogen makes conditions favorable for some invasive species and threatens biodiversity of Mediterranean ecosystems[231,232]

Thus, acidification and solubility of ambient dust is an important phenomenon that potentially affects food security, forest growth, and other critical environmental issues of importance to the increasingly arid Eastern Mediterranean Region. Accurate predictions of dust conversion processes are thus paramount to rational land and marine ecosystem management.

From a health perspective, dust events were often associated with enhanced airborne micro-organisms. This preliminary study showed a significant increase in the total count per unit sampled air (m^3) of fungi and of a special type of bacteria; *Bacillus Cereus*, commonly

encountered in the region[154], during dust storms. Further investigation in this regard will continue in our labs.

BIBLIOGRAPHY

(1) Finlayson-Pitts, B. J.; Pitts, J. N. *Chemistry of the Upper and Lower Atmosphere: Theory, Experiments and Applications*; Academic Press: San Diego, CA, 2000.

(2) de Miranda, R. M.; de Fátima Andrade, M.; Worobiec, A.; Grieken, R. V. *Atmospheric environment* **2002**, *36*, 345.

(3) Colbeck, I. *Environmental chemistry of aerosols*; Wiley Online Library, 2008.

(4) Ooki, A.; Uematsu, M. *Journal of Geophysical Research: Atmospheres* **2005**, *110*, D03201.

(5) Sullivan, R.; Guazzotti, S.; Sodeman, D.; Prather, K. *Atmospheric Chemistry and Physics* **2007**, *7*, 1213.

(6) Seinfeld, J. H.; Pandis, S. N. *Atmospheric chemistry and physics: from air pollution to climate change*; John Wiley & Sons, 2012.

(7) Dada, L.; Mrad, R.; Siffert, S.; Saliba, N. *Journal of Aerosol Science* **2013**, *66*, 187.

(8) Krueger, B. J.; Grassian, V. H.; Cowin, J. P.; Laskin, A. *Atmospheric Environment* **2004**, *38*, 6253.

(9) Usher, C. R.; Michel, A. E.; Grassian, V. H. *Chemical reviews* **2003**, *103*, 4883.

(10) Middleton, N. J. *Journal of Arid Environments* **1986**, *10*, 83.

(11) Alpert, P.; Osetinsky, I.; Ziv, B.; Shafir, H. *International Journal of Climatology* **2004**, *24*, 1013.

(12) Alpert, P.; Osetinsky, I.; Ziv, B.; Shafir, H. *International Journal of Climatology* **2004b**, *24*, 1001.

(13) Goudie, A. S.; Middleton, N. J. *Earth-Science Reviews* **2001**, *56*, 179.

(14) Ganor, E.; Osetinsky, I.; Stupp, A.; Alpert, P. *Journal of Geophysical Research D: Atmospheres* **2010**, *115*, art. no. D07201.

(15) Lelieveld, J.; Hadjinicolaou, P.; Kostopoulou, E.; Giannakopoulos, C.; Pozzer, A.; Tanarhte, M.; Tyrlis, E. *Regional Environmental Change* **2013**, 1.

(16) Kubilay, N.; Nickovic, S.; Moulin, C.; Dulac, F. *Atmospheric Environment* **2000**, *34*, 1293.

(17) Ganor, E.; Stupp, A.; Alpert, P. *Atmospheric Environment* **2009**, *43*, 5463.

(18) Baalbaki, R.; Al-Assaad, K.; Mehanna, C.-J.; Saliba, N. A.; Katurji, M.; Roumié, M. *Journal of the Air & Waste Management Association* **2013**, *63*, 327.

(19) Jaafar, M.; Baalbaki, R.; Mrad, R.; Daher, N.; Shihadeh, A.; Sioutas, C.; Saliba, N. A. *Science of the Total Environment* **2014**.

(20) Saliba, N.; Massoud, R. In *Urban Airborne Particulate Matter*; Zereini, F., Wiseman, C. L. S., Eds.; Springer Berlin Heidelberg: 2011, p 3.

(21) Saliba, N.; Moussa, S.; El Tayyar, G. *Atmospheric Chemistry and Physics Discussions* **2014**, *14*, 4827.

(22) Saliba, N. A.; Chamseddine, A. *Atmospheric Environment* **2012**, *46*, 256.

(23) Saliba, N. A.; El Jam, F.; El Tayar, G.; Obeid, W.; Roumie, M. *Atmospheric Research* **2010**, *97*, 106.

(24) Ooki, A.; Uematsu, M. *Journal of Geophysical Research: Atmospheres (1984–2012)* **2005**, *110*.

(25) Tang, I. N. *Journal of Geophysical Research: Atmospheres (1984–2012)* **1996**, *101*, 19245.

(26) Tegen, I. *Quaternary Science Reviews* **2003**, *22*, 1821.

(27) Buseck, P. R.; POsfai, M. *Proceedings of the National Academy of Sciences* **1999**, *96*, 3372.

(28) Perraud, V.; Bruns, E. A.; Ezell, M. J.; Johnson, S. N.; Yu, Y.; Alexander, M. L.; Zelenyuk, A.; Imre, D.; Chang, W. L.; Dabdub, D. *Proceedings of the National Academy of Sciences* **2012**, *109*, 2836.

(29) Topinka, J.; Milcova, A.; Schmuczerova, J.; Krouzek, J.; Hovorka, J. *Mutation Research - Genetic Toxicology and Environmental Mutagenesis* **2013**, *754*, 1.

(30) Wu, C. C.; Liu, H. M. *Archives of Environmental and Occupational Health* **2014**, *69*, 131.

(31) Zhu, Y.; Yang, L.; Yuan, Q.; Yan, C.; Dong, C.; Meng, C.; Sui, X.; Yao, L.; Yang, F.; Lu, Y.; Wang, W. *Science of the Total Environment* **2014**, *466-467*, 357.

(32) Dulac, F.; Buat-Menard, P.; Arnold, M.; Ezat, U.; Martin, D. *Journal of Geophysical Research* **1987**, *92*, 8437.

(33) Bergametti, G.; Dutot, A. L.; Buat-Menard, P.; Losno, R.; Remoudaki, E. *TELLUS, SER. B. CHEM. PHYS. METEOROL.* **1989**, *41*, 353.

(34) Migon, C.; Morelli, J.; Nicolas, E.; Copin-Montegut, G. *Science of the Total Environment* **1991**, *105*, 135.

(35) Sandroni, V.; Migon, C. *Science of the Total Environment* **1997**, *196*, 83.

(36) Chester, R.; Nimmo, M.; Preston, M. R. *Marine Chemistry* **1999**, *68*, 15.

(37) Querol, X.; Alastuey, A.; Rodriguez, S.; Plana, F.; Mantilla, E.; Ruiz, C. R. *Atmospheric Environment* **2001a**, *35*, 845.

(38) Querol, X.; Alastuey, A.; Rodriguez, S.; Plana, F.; Ruiz, C. R.; Cots, N.; Massagué, G.; Puig, O. *Atmospheric Environment* **2001b**, *35*, 6407.

(39) Mamane, Y.; Ganor, E.; Donagi, A. E. *Water, Air, & Soil Pollution* **1980**, *VOL.14*, 29.

(40) Ganor, E. *Atmospheric Environment - Part A General Topics* **1991**, *25 A*, 2657.

(41) Ganor, E.; Foner, H. A.; Brenner, S.; Neeman, E.; Lavi, N. *Atmospheric Environment - Part A General Topics* **1991**, *25 A*, 2665.

(42) Mihalopoulos, N.; Stephanou, E.; Kanakidou, M.; Pilitsidis, S.; Bousquet, P. *Tellus, Series B: Chemical and Physical Meteorology* **1997**, *49*, 314.

(43) Güllü, G. H.; Ölmez, I.; Tuncel, G. *Spectrochimica acta, Part B: Atomic spectroscopy* **2000**, *55*, 1135.

(44) Chabas, A.; Lefèvre, R. A. *Atmospheric Environment* **2000**, *34*, 225.

(45) Yatin, M.; Tuncel, S.; Aras, N. K.; Olmez, I.; Aygun, S.; Tuncel, G. *Atmospheric Environment* **2000**, *34*, 1305.

(46) Soner Erduran, M.; Tuncel, S. G. *Science of the Total Environment* **2001**, *281*, 205.

(47) Manoli, E.; Voutsa, D.; Samara, C. *Atmospheric Environment* **2002**, *36*, 949.

(48) Thomaidis, N. S.; Bakeas, E. B.; Siskos, P. A. *Chemosphere* **2003**, *52*, 959.

(49) Graham, B.; Falkovich, A. H.; Rudich, Y.; Maenhaut, W.; Guyon, P.; Andreae, M. O. *Atmospheric Environment* **2004**, *38*, 1593.

(50) Manalis, N.; Grivas, G.; Protonotarios, V.; Moutsatsou, A.; Samara, C.; Chaloulakou, A. *Chemosphere* **2005**, *60*, 557.

(51) Saliba, N. A.; Chamseddine, A. *Atmospheric Environment* **2012**, *46*, 256.

(52) Daher, N.; Saliba, N. A.; Shihadeh, A. L.; Jaafar, M.; Baalbaki, R.; Sioutas, C. *Atmospheric Environment* **2013**, *80*, 96.

(53) Draxler, R. R.; Rolph, G. D. **2013**.

(54) Rolph, G. D. **2013**.

(55) Notaro, M.; Alkolibi, F.; Fadda, E.; Bakhrjy, F. *Journal of Geophysical Research: Atmospheres* **2013**, *118*, 6028.

(56) Tsai, J.-H.; Chang, L.-P.; Chiang, H.-L. *Environmental Science and Pollution Research* **2013**, *20*, 4587.

(57) McInnes, L.; Covert, D.; Quinn, P.; Germani, M. *Journal of Geophysical Research: Atmospheres (1984–2012)* **1994**, *99*, 8257.

(58) Fu, F.; Watanabe, K.; Yabuki, S.; Akagi, T. *Journal of Geophysical Research: Atmospheres (1984–2012)* **2004**, *109*.

(59) Wall, S. M.; John, W.; Ondo, J. L. *Atmospheric Environment (1967)* **1988**, *22*, 1649.

(60) Ten Harkel, M. *Atmospheric Environment* **1997**, *31*, 417.

(61) Pakkanen, T. A. *Atmospheric Environment* **1996**, *30*, 2475.

(62) Zhuang, H.; Chan, C. K.; Fang, M.; Wexler, A. S. *Atmospheric Environment* **1999**, *33*, 4223.

(63) Chang, S.; McDonald-Buller, E.; Kimura, Y.; Yarwood, G.; Neece, J.; Russell, M.; Tanaka, P.; Allen, D. *Atmospheric Environment* **2002**, *36*, 4991.

(64) Atkinson, R. *Journal of Physical and Chemical Reference Data* **1997**, *26*, 215.

(65) Atkinson, R.; Baulch, D.; Cox, R.; Crowley, J.; Hampson, R.; Hynes, R.; Jenkin, M.; Rossi, M.; Troe, J.; Subcommittee, I. *Atmospheric Chemistry and Physics* **2006**, *6*, 3625.

(66) Chang, S.; Allen, D. T. *Environmental science & technology* **2006**, *40*, 251.

(67) Eldering, A.; Solomon, P. A.; Salmon, L. G.; Fall, T.; Cass, G. R. *Atmospheric Environment. Part A. General Topics* **1991**, *25*, 2091.

(68) Laskin, A.; Gaspar, D. J.; Wang, W.; Hunt, S. W.; Cowin, J. P.; Colson, S. D.; Finlayson-Pitts, B. J. *Science* **2003**, *301*, 340.

(69) Mamane, Y.; Gottlieb, J. *Atmospheric Environment. Part A. General Topics* **1992**, *26*, 1763.

(70) Ottley, C.; Harrison, R. M. *Atmospheric Environment. Part A. General Topics* **1992**, *26*, 1689.

(71) Ravishankara, A. *Proceedings of the National Academy of Sciences* **2009**, *106*, 13639.

(72) Oldfield, S.; Allen, D.

(73) Pakkanen, T. A.; Kerminen, V.-M.; Korhonen, C. H.; Hillamo, R. E.; Aarnio, P.; Koskentalo, T.; Maenhaut, W. *Atmospheric Environment* **2001**, *35*, 4593.

(74) Heshun, D. *Acta Mineralogica Sinica* **2005**, *25*, 135.

(75) Silva, P. J.; Liu, D.-Y.; Noble, C. A.; Prather, K. A. *Environmental science & technology* **1999**, *33*, 3068.

(76) Li, J.; Pósfai, M.; Hobbs, P. V.; Buseck, P. R. *Journal of Geophysical Research: Atmospheres* **2003**, *108*, 8484.

(77) Ro, C. U.; Hwang, H.; Kim, H.; Chun, Y.; Van Grieken, R. *Environmental Science and Technology* **2005**, *39*, 1409.

(78) Engelen, K.; Lefebvre, M. H.; Hubin, A. *Propellants, Explosives, Pyrotechnics* **2002**, *27*, 290.

(79) Krueger, B. J.; Grassian, V. H.; Laskin, A.; Cowin, J. P. *Geophysical Research Letters* **2003**, *30*.

(80) Laskin, A.; Wietsma, T. W.; Krueger, B. J.; Grassian, V. H. *Journal of Geophysical Research: Atmospheres (1984–2012)* **2005**, *110*.

(81) Kelly, J. T.; Chuang, C. C.; Wexler, A. S. *Atmospheric Environment* **2007**, *41*, 2904.

(82) Finlayson-Pitts, B. J.; Wingen, L.; Sumner, A. L.; Syomin, D.; Ramazan, K. A. *Physical Chemistry Chemical Physics* **2003**, *5*, 223.

(83) Pathak, R. K.; Wang, T.; Wu, W. S. *Atmospheric Environment* **2011**, *45*, 1183.

(84) Kadowaki, S. *Atmospheric Environment (1967)* **1977**, *11*, 671.

(85) Meng, Z.; Seinfeld, J. H. *Aerosol Science and Technology* **1994**, *20*, 253.

(86) Pandey, S. K.; Tripathi, B.; Mishra, V.; Prajapati, S. *Chemosphere* **2006**, *63*, 49.

(87) Samara, C.; Tsitouridou, R. *Water, Air, & Soil Pollution* **2000**, *120*, 71.

(88) Hitchcock, D. R.; Spiller, L. L.; Wilson, W. E. *Atmospheric Environment (1967)* **1980**, *14*, 165.

(89) Theodosi, C.; Grivas, G.; Zarmpas, P.; Chaloulakou, A.; Mihalopoulos, N. *Atmospheric Chemistry and Physics* **2011**, *11*, 11895.

(90) Sievering, H.; Boatman, J.; Gorman, E.; Kim, Y.; Anderson, L.; Ennis, G.; Luria, M.; Pandis, S. *Nature* **1992**, *360*, 571.

(91) Finlayson-Pitts, B. J.; Pitts Jr, J. N. *Chemistry of the upper and lower atmosphere: theory, experiments, and applications*; Access Online via Elsevier, 1999.

(92) Stelson, A.; Seinfeld, J. *Atmospheric Environment (1967)* **1982**, *16*, 983.

(93) Ellis, R.; Murphy, J.; Markovic, M.; VandenBoer, T.; Makar, P.; Brook, J.; Mihele, C. *Atmospheric Chemistry and Physics Discussions* **2010**, *10*, 21895.

(94) Navarro, S. L.; Peterson, S.; Chen, C.; Makar, K. W.; Schwarz, Y.; King, I. B.; Li, S. S.; Li, L.; Kestin, M.; Lampe, J. W. *Cancer Prevention Research* **2009**, *2*, 345.

(95) Fangmeier, A.; Hadwiger-Fangmeier, A.; Van der Eerden, L.; Jäger, H.-J. *Environmental pollution* **1994**, *86*, 43.

(96) Bobbink, R. *New Phytologist* **1998**, *139*, 161.

(97) Galloway, J. N.; Aber, J. D.; Erisman, J. W.; Seitzinger, S. P.; Howarth, R. W.; Cowling, E. B.; Cosby, B. J. *Bioscience* **2003**, *53*, 341.

(98) Krupa, S. *Environmental pollution* **2003**, *124*, 179.

(99) Sillanpää, M.; Hillamo, R.; Saarikoski, S.; Frey, A.; Pennanen, A.; Makkonen, U.; Spolnik, Z.; Van Grieken, R.; Braniš, M.; Brunekreef, B. *Atmospheric Environment* **2006**, *40*, 212.

(100) Shen, J.; Liu, X.; Zhang, Y.; Fangmeier, A.; Goulding, K.; Zhang, F. *Atmospheric Environment* **2011**, *45*, 5033.

(101) Trebs, I.; Metzger, S.; Meixner, F. X.; Helas, G.; Hoffer, A.; Rudich, Y.; Falkovich, A. H.; Moura, M. A.; da Silva, R. S.; Artaxo, P. *Journal of Geophysical Research: Atmospheres (1984–2012)* **2005**, *110*.

(102) Tsai, Y. I.; Cheng, M. T. *Science of the Total Environment* **1999**, *231*, 37.

(103) Kant Pathak, R.; Chan, C. K. *Atmospheric Environment* **2005**, *39*, 1597.

(104) Shaka, H.; Saliba, N. A. *Atmospheric Environment* **2004**, *38*, 523.

(105) Kouyoumdjian, H.; Saliba, N. *Atmospheric Chemistry and Physics* **2006**, *6*, 1865.

(106) Saxena, P.; Mueller, P. K.; Kim, y. P.; Seinfeld, J. H.; Koutrakis, P. *Aerosol science and technology* **1993**, *19*, 279.

(107) Schwab, J. J.; Felton, H.; Demerjian, K. L. *Journal of Geophysical Research: Atmospheres (1984–2012)* **2004**, *109*.

(108) Kerminen, V.-M.; Hillamo, R.; Teinilä, K.; Pakkanen, T.; Allegrini, I.; Sparapani, R. *Atmospheric Environment* **2001**, *35*, 5255.

(109) Yao, X.; Yan Ling, T.; Fang, M.; Chan, C. K. *Atmospheric Environment* **2006**, *40*, 2835.

(110) Lightowlers, P. J.; Cape, J. N. *Atmospheric Environment (1967)* **1988**, *22*, 7.

(111) Russell, A. G.; McRae, G. J.; Cass, G. R. In *Air Pollution Modeling and its Application III*; Springer: 1984, p 539.

(112) Russell, A. G.; McRae, G. J.; Cass, G. R. *Atmospheric Environment (1967)* **1985**, *19*, 893.

(113) Derwent, R. G.; Nodopt, K. **1986**.

(114) Behera, S. N.; Betha, R.; Balasubramanian, R. *Aerosol and Air Quality Research* **2013**, *13*, 1282.

(115) Aneja, V. P.; Agarwal, A.; Roelle, P. A.; Phillips, S. B.; Tong, Q.; Watkins, N.; Yablonsky, R. *Environment International* **2001**, *27*, 35.

(116) Weimin, S. *Iron and Steel* **1999**, *7*.

(117) Valente, O. S.; da Silva, M. J.; Pasa, V. M. D.; Belchior, C. R. P.; Sodré, J. R. *Fuel* **2010**, *89*, 3637.

(118) Khoder, M. *Chemosphere* **2002**, *49*, 675.

(119) Ma, J.; Liu, Y. C.; Han, C.; Ma, Q.; Liu, C.; He, H. *Journal of Environmental Sciences* **2013**, *25*, 326.

(120) Ullerstam, M.; Johnson, M. S.; Vogt, R.; Ljungstrom, E. *Atmospheric Chemistry and Physics* **2003**, *3*, 2043.

(121) Underwood, G. M.; Miller, T. M.; Grassian, V. H. *Journal of Physical Chemistry A* **1999**, *103*, 6184.

(122) Underwood, G. M.; Song, C. H.; Phadnis, M.; Carmichael, G. R.; Grassian, V. H. *JOURNAL OF GEOPHYSICAL RESEARCH* **2001**, *D16*, 18.

(123) Yu, Y.; Galle, B.; Panday, A.; Hodson, E.; Prinn, R.; Wang, S. *Atmospheric Chemistry and Physics* **2009**, *9*, 6401.

(124) Liu, C.; Ma, Q.; Liu, Y. C.; Ma, J.; He, H. *Physical Chemistry Chemical Physics* **2012**, *14*, 1668.

(125) Beaumont, S. K.; Gustafsson, R. J.; Lambert, R. M. *Chemical Physics and Physical Chemistry* **2009**, *10*, 331.

(126) Langridge, J. M.; Gustafsson, R. J.; Griffiths, P. T.; Anthony Cox, R.; Lambert, R. M.; Jones, R. L. *Atmospheric Environment* **2009**, *43*, 5128.

(127) Ndour, M.; D'Anna, B.; George, C.; Ka, O.; Balkanski, Y.; Kleffmann, J.; Stemmler, K.; Ammann, M. *Geophysical Research Letters* **2008**, *35*.

(128) Dentener, F. J.; Carmichael, G. R.; Zhang, Y.; Lelieveld, J.; Crutzen, P. J. *Journal of Geophysical Research: Atmosphere* **1996**, *101*, 22869−22889.

(129) Guo, Y. T.; Zhang, J.; Wang, S. G.; She, F.; Li, X. *Journal of Atmospheric Chemistry* **2011**, *68*, 299−316.

(130) Usher, C. R.; Michel, A. E.; Grassian, V. H. *Chemical Reviews* **2003**, *103*, 4883−4939.

(131) Ullerstam, M.; Vogt, R.; Langer, S.; Ljungstrom, E. *Physical Chemistry Chemical Physics* **2002**, *4*, 4694.

(132) Borerisen, C.; Kitether, U.; Schear, V.; Vogt, R.; Zellner, R. *journal of Physical Chemistry A* **2000**, *104*, 5036.

(133) Phillips, L. F. *Physical Chemistry Chemical Physics* **2013**, *15*, 10749.

(134) Wu, F. C.; Xie, P. H.; Li, A.; Chan, K. L.; Hartl, A.; Wang, Y.; Si, F. Q.; Zeng, Y.; Qin, M.; Xu, J.; Liu, J. G.; Liu, W. Q.; Wenig, M. *Atmospheric Measurement Techniques* **2013**, *6*, 2277.

(135) Wang, S. G.; Ackermann, R.; Spicer, C. W.; Fast, J. D.; Schmeling, M.; Stutz, J. *Geophysical Research Letters* **2003**, *30*, doi:10.1029/2003GL017014.

(136) Zhu, S.; Butler, T.; Sander, R.; Ma, J.; Lawrence, M. G. *Atmospheric Chemistry and Physics* **2010**, *10*, 3855.

(137) Draxler, R. R.; Rolph, G. D. In *NOAA Air Resources Laboratory,* Silver Spring, MD, 2013.

(138) Ma, Q.; Liu, Y. C.; He, H. *Journal of Physical Chemistry A* **2008**, *112*, 6630.

(139) Tindale, N. W.; Pease, P. P. *Deep-Sea Research Part II: Topical Studies in Oceanography* **1999**, *46*, 1577.

(140) Kutiel, H.; Furman, H. *Indoor and Built Environment* **2003**, *12*, 419.

(141) Baalbaki, R.; Al-Assaad, K.; Mehanna, C. J.; Saliba, N. A.; Katurji, M.; Roumié, M. *Journal of the Air and Waste Management Association* **2013**, *63*, 327.

(142) Notaro, M.; Alkolibi, F.; Fadda, E.; Bakhrjy, F. *Journal of Geophysical Research D: Atmospheres* **2013**, *118*, 6028.

(143) Massoud, R.; Shihadeh, A. L.; Roumié, M.; Youness, M.; Gerard, J.; Saliba, N.; Zaarour, R.; Abboud, M.; Farah, W.; Saliba, N. A. *Atmospheric Research* **2011**, *101*, 893.

(144) Saliba, N. A.; Kouyoumdjian, H.; Roumié, M. *Atmospheric Environment* **2007**, *41*, 6497.

(145) Saliba, N. A.; Moussa, S.; Salame, H.; El-Fadel, M. *Atmospheric Environment* **2006**, *40*, 3263.

(146) MOE/UNDP/ECODIT In *State and Trends of the Lebanese Environment 2010* Lebanon, 2011, p 355.

(147) Senlin, L.; Zhenkun, Y.; Xiaohui, C.; Minghong, W.; Guoying, S.; Jiamo, F.; Paul, D. *Atmospheric Environment* **2008**, *42*, 7205.

(148) Ganor, E.; Altshuller, S.; Foner, H. A.; Brenner, S.; Gabbay, J. *Water, Air, and Soil Pollution* **1988**, *42*, 241.

(149) Coz, E.; Gomez-Moreno, F. J.; Pujadas, M.; Casuccio, G. S.; Lersch, T. L.; Artinano, B. *Atmospheric Environment* **2009**, *43*, 1850.

(150) Furutani, H.; Meguro, A.; Iguchi, H.; Uematsu, M. *Geophysical Research Letters* **2010**, *37*, L03805.

(151) Laskin, A.; Iedema, M. J.; Ichkovich, A.; Graber, E. R.; Taraniuk, I.; Rudich, Y. *Faraday Discussions* **2005**, *130*, 453.

(152) Ahlskog, M.; Seynaeve, E.; Vullers, R. J. M.; Van Haesendonck, C.; Fonseca, A.; Hernadi, K.; B.Nagy, J. *Chemical Physics Letters* **1999**, *300*, 202.

(153) Becagli, S.; Scarchilli, C.; Traversi, R.; Dayan, U.; Severi, M.; Frosini, D.; Vitale, V.; Mazzola, M.; Lupi, A.; Nava, S.; Udisti, R. *Atmospheric Environment* **2012**, *52*, 98.

(154) Goudarzi, G.; Shirmardi, M.; Khodarahmi, F.; Hashemi-Shahraki, A.; Alavi, N.; Ankali, K. A.; Babaei, A. A.; Soleimani, Z.; Marzouni, M. B. *Aerobiologia* **2014**.

(155) Wang, W.; Ma, Y.; Ma, X.; Wu, F.; Ma, X.; An, L.; Feng, H. *International Biodeterioration & Biodegradation* **2010**, *64*, 309.

(156) Elbert, W.; Taylor, P.; Andreae, M.; Pöschl, U. *Atmospheric Chemistry and Physics* **2007**, *7*, 4569.

(157) Jaenicke, R. *Science* **2005**, *308*, 73.

(158) Jaenicke, R.; Matthias-Maser, S.; Gruber, S. *Environmental Chemistry* **2007**, *4*, 217.

(159) Jones, A. M.; Harrison, R. M. *Science of the total environment* **2004**, *326*, 151.

(160) Gregory, P. *Proceedings of the Royal Society of London. Series B. Biological Sciences* **1971**, *177*, 469.

(161) Pasteur, L. *Suite à une précédente communication relative aux générations dites spontanées*; Mallet-Bachelier, 1860.

(162) Fang, Z.; Ouyang, Z.; Zheng, H.; Wang, X.; Hu, L. *Microbial ecology* **2007**, *54*, 487.

(163) Ho, H.-M.; Rao, C. Y.; Hsu, H.-H.; Chiu, Y.-H.; Liu, C.-M.; Chao, H. *Atmospheric Environment* **2005**, *39*, 5839.

(164) Jeon, E. M.; Kim, H. J.; Jung, K.; Kim, J. H.; Kim, M. Y.; Kim, Y. P.; Ka, J. O. *Atmospheric Environment* **2011**, *45*, 4313.

(165) Burrows, S.; Elbert, W.; Lawrence, M.; Pöschl, U. *Atmospheric Chemistry and Physics* **2009**, *9*, 9263.

(166) Schnell, R.; Vali, G. *Nature* **1972**, *236*, 163.

(167) Schnell, R.; Vali, G. **1973**.

(168) Yankofsky, S.; Levin, Z.; Bertold, T.; Sandlerman, N. *Journal of applied meteorology* **1981a**, *20*, 1013.

(169) Amato, P.; Demeer, F.; Melaouhi, A.; Fontanella, S.; Martin-Biesse, A.-S.; Sancelme, M.; Laj, P.; Delort, A.-M. *Atmospheric Chemistry and Physics* **2007a**, *7*, 4159.

(170) Amato, P.; Ménager, M.; Sancelme, M.; Laj, P.; Mailhot, G.; Delort, A.-M. *Atmospheric Environment* **2005**, *39*, 4143.

(171) Amato, P.; Parazols, M.; Sancelme, M.; Laj, P.; Mailhot, G.; Delort, A. M. *FEMS microbiology ecology* **2007b**, *59*, 242.

(172) Ariya, P.; Sun, J.; Eltouny, N.; Hudson, E.; Hayes, C.; Kos, G. *International Reviews in Physical Chemistry* **2009**, *28*, 1.

(173) Ariya, P. A.; Nepotchatykh, O.; Ignatova, O.; Amyot, M. *Geophysical Research Letters* **2002**, *29*, 34.

(174) Bauer, H.; Giebl, H.; Hitzenberger, R.; Kasper-Giebl, A.; Reischl, G.; Zibuschka, F.; Puxbaum, H. *Journal of Geophysical Research: Atmospheres (1984–2012)* **2003**, *108*.

(175) Christner, B. C.; Morris, C. E.; Foreman, C. M.; Cai, R.; Sands, D. C. *Science* **2008**, *319*, 1214.

(176) Deguillaume, L.; Leriche, M.; Amato, P.; Ariya, P.; Delort, A.-M.; Pöschl, U.; Chaumerliac, N.; Bauer, H.; Flossmann, A.; Morris, C. *Biogeosciences Discussions* **2008**, *5*.

(177) Diehl, K.; Simmel, M.; Wurzler, S. *Journal of Geophysical Research: Atmospheres (1984–2012)* **2006**, *111*.

(178) Junge, K.; Swanson, B. *Biogeosciences* **2008**, *5*.

(179) Möhler, O.; DeMott, P.; Vali, G.; Levin, Z. *Biogeosciences Discussions* **2007**, *4*.

(180) Möhler, O.; Georgakopoulos, D.; Morris, C.; Benz, S.; Ebert, V.; Hunsmann, S.; Saathoff, H.; Schnaiter, M.; Wagner, R. *Biogeosciences Discussions* **2008**, *5*.

(181) Morris, C.; Georgakopoulos, D.; Sands, D. In *Journal de Physique IV (Proceedings)*; EDP sciences: 2004; Vol. 121, p 87.

(182) Mortazavi, R.; Hayes, C. T.; Ariya, P. A. *Environmental chemistry* **2008**, *5*, 373.

(183) Pratt, K. A.; DeMott, P. J.; French, J. R.; Wang, Z.; Westphal, D. L.; Heymsfield, A. J.; Twohy, C. H.; Prenni, A. J.; Prather, K. A. *Nature Geoscience* **2009**, *2*, 398.

(184) Prenni, A. J.; Petters, M. D.; Kreidenweis, S. M.; Heald, C. L.; Martin, S. T.; Artaxo, P.; Garland, R. M.; Wollny, A. G.; Pöschl, U. *Nature Geoscience* **2009**, *2*, 402.

(185) Sands, D.; Langhans, V.; Scharen, A.; De Smet, G. *Idojaras* **1982**.

(186) Sands, D. C.; Georgakopoulos, D. G. *Simulation* **1991**, *56*, 295.

(187) Sun, J.; Ariya, P. A. *Atmospheric Environment* **2006**, *40*, 795.

(188) Yankofsky, S. A.; Levin, Z.; Moshe, A. *Current microbiology* **1981b**, *5*, 213.

(189) Griffin, D. W. *Clinical microbiology reviews* **2007a**, *20*, 459.

(190) Griffin, D. W.; Kubilay, N.; Koçak, M.; Gray, M. A.; Borden, T. C.; Shinn, E. A. *Atmospheric Environment* **2007b**, *41*, 4050.

(191) Hua, N.-P.; Kobayashi, F.; Iwasaka, Y.; Shi, G.-Y.; Naganuma, T. *Aerobiologia* **2007**, *23*, 291.

(192) Kellogg, C. A.; Griffin, D. W. *Trends in ecology & evolution* **2006**, *21*, 638.

(193) Yamaguchi, N.; Park, J.; Kodama, M.; Ichijo, T.; Baba, T.; Nasu, M. *Microbes and Environments* **2014**, *29*, 82.

(194) Schlesinger, P.; Mamane, Y.; Grishkan, I. *Aerobiologia* **2006**, *22*, 259.

(195) Grishkan, I.; Schlesinger, P.; Mamane, Y. *Aerobiologia* **2012**, *28*, 557.

(196) Burger, H. *Journal of Allergy and Clinical Immunology* **1990**, *86*, 687.

(197) Alpert, F.; Ganor, E. *Journal of Geophysical Research* **1993**, *98*, 7339.

(198) Dayan, U.; Heffter, J.; Miller, J.; Gutman, G. *Journal of Applied Meteorology* **1991**, *30*, 1185.

(199) Escudero, M.; Castillo, S.; Querol, X.; Avila, A.; Alarcón, M.; Viana, M. M.; Alastuey, A.; Cuevas, E.; Rodríguez, S. *Journal of Geophysical Research D: Atmospheres* **2005**, *110*, 1.

(200) Escudero, M.; Stein, A. F.; Draxler, R. R.; Querol, X.; Alastuey, A.; Castillo, S.; Avila, A. *Atmospheric Research* **2011**, *99*, 518.

(201) Kassaify, Z.; Najjar, M.; Toufeili, I.; Malek, A. *Eastern Mediterranean Health Journal* **2010**, *16*.

(202) Manual, B.; 8th ed.; ADMINISTRATION, F. D., Ed.; AOAC International: 1995.

(203) Kassaify, Z. G.; El Hajj, R. H.; Hamadeh, S. K.; Zurayk, R.; Barbour, E. K. *Journal of Coastal Research* **2009**, 469.

(204) Heidelberg, J.; Shahamat, M.; Levin, M.; Rahman, I.; Stelma, G.; Grim, C.; Colwell, R. *Applied and Environmental Microbiology* **1997**, *63*, 3585.

(205) Lighthart, B.; Tong, Y. *Aerobiologia* **1998**, *14*, 325.

(206) Peccia, J.; Hernandez, M. *Atmospheric Environment* **2006**, *40*, 3941.

(207) Soleimani, Z.; Goudarzi, G.; Naddafi, K.; Sadeghinejad, B.; Latifi, S. M.; Parhizgari, N.; Alavi, N.; Babaei, A. A.; Akhoond, M. R.; Khaefi, M. *Aerobiologia* **2013**, *29*, 279.

(208) Raisi, L.; Aleksandropoulou, V.; Lazaridis, M.; Katsivela, E. *Aerobiologia* **2013**, *29*, 233.

(209) Li, M.; Qi, J.; Zhang, H.; Huang, S.; Li, L.; Gao, D. *Science of The Total Environment* **2011**, *409*, 3812.

(210) Pyrri, I.; Kapsanaki-Gotsi, E. *Aerobiologia* **2012**, *28*, 249.

(211) Alghamdi, M. A.; Shamy, M.; Redal, M. A.; Khoder, M.; Awad, A. H.; Elserougy, S. *Science of The Total Environment* **2014**, *479*, 109.

(212) Lighthart, B. *Atmospheric environment* **1999**, *33*, 611.

(213) Maron, P. A.; Mougel, C.; H Lejon, D. P.; Carvalho, E.; Bizet, K.; Marck, G.; Cubito, N.; Lemanceau, P.; Ranjard, L. *Atmospheric Environment* **2006**, *40*, 8074.

(214) Stetzenbach, L.; Hurst, C.; Crawford, R.; Garland, J.; Lipson, D.; Mills, A. *Manual of environmental microbiology* **2007**, 925.

(215) Laine, M. M.; Jørgensen, K. S.; Kiviranta, H.; Vartiainen, T.; Jokela, J. K.; Adibi, A.; Salkinoja-Salonen, M. *Bioremediation Journal* **1999**, *3*, 47.

(216) Shoreit, A. A.; Ismail, M. A. *Zentralblatt fur Mikrobiologie* **1992**, *147*, 541.

(217) Bauer, H.; Kasper-Giebl, A.; Zibuschka, F.; Hitzenberger, R.; Kraus, G. F.; Puxbaum, H. *Analytical Chemistry* **2001**, *74*, 91.

(218) Boreson, J.; Dillner, A. M.; Peccia, J. *Atmospheric Environment* **2004**, *38*, 6029.

(219) Kaushik, R.; Balasubramanian, R. *Atmospheric Environment* **2012**, *46*, 131.

(220) Hospodsky, D.; Yamamoto, N.; Peccia, J. *Applied and Environmental Microbiology* **2010**, *76*, 7004.

(221) Derimian, Y.; Karnieli, A.; Kaufman, Y. J.; Andreae, M. O.; Andreae, T. W.; Dubovik, O.; Maenhaut, W.; Koren, I.; Holben, B. N. *Journal of Geophysical Research: Atmospheres* **2006**, *111*, D05205.

(222) Israelevich, P.; Ganor, E.; Alpert, P.; Kishcha, P.; Stupp, A. *Journal of Geophysical Research: Atmospheres* **2012**, *117*, D02205.

(223) Erel, Y.; Dayan, U.; Rabi, R.; Rudich, Y.; Stein, M. *Environmental Science & Technology* **2006**, *40*, 2996.

(224) Oakes, M.; Ingall, E. D.; Lai, B.; Shafer, M. M.; Hays, M. D.; Liu, Z. G.; Russell, A. G.; Weber, R. J. *Environmental Science & Technology* **2012**, *46*, 6637.

(225) Dentener, F. J.; Carmichael, G. R.; Zhang, Y.; Lelieveld, J.; Crutzen, P. J. *Journal of Geophysical Research: Atmospheres (1984–2012)* **1996**, *101*, 22869.

(226) Rastogi, N.; Sarin, M. M. *Geophysical Research Letters* **2006**, *33*, L23815.

(227) Weber, R. J.; Sullivan, A. P.; Peltier, R. E.; Russell, A.; Yan, B.; Zheng, M.; De Gouw, J.; Warneke, C.; Brock, C.; Holloway, J. S. *Journal of Geophysical Research: Atmospheres (1984–2012)* **2007**, *112*.

(228) Meskhidze, N.; Chameides, W. L.; Nenes, A. *Journal of Geophysical Research: Atmospheres* **2005**, *110*, D03301.

(229) Baker, A. R.; Kelly, S. D.; Biswas, K. F.; Witt, M.; Jickells, T. D. *Geophysical Research Letters* **2003**, *30*, 2296.

(230) Driscoll, C. T.; Driscoll, K. M.; Mitchell, M. J.; Raynal, D. J. *Environmental Pollution* **2003**, *123*, 327.

(231) Bleeker, A.; Hicks, W. K.; Dentener, F.; Galloway, J.; Erisman, J. W. *Environmental Pollution* **2011**, *159*, 2280.

(232) Bobbink, R.; Hicks, K.; Galloway, J.; Spranger, T.; Alkemade, R.; Ashmore, M.; Bustamante, M.; Cinderby, S.; Davidson, E.; Dentener, F.; Emmett, B.; Erisman, J. W.; Fenn, M.; Gilliam, F.; Nordin, A.; Pardo, L.; De Vries, W. *Ecological Applications* **2010**, *20*, 30.